ARMY RESEARCH LABORATORY

Enhancing the High Temperature Capability of Nanocrystalline Alloys: Utilizing Thermodynamic Stability Maps to Mitigate Grain Growth Through Solute Selection

by Mark A. Tschopp, Kristopher A. Darling, Brian K. VanLeeuwen, Mark A. Atwater, and Zi-Kui Liu

ARL-TR-6743 December 2013

NOTICES

Disclaimers

The findings in this report are not to be construed as an official Department of the Army position unless so designated by other authorized documents.

Citation of manufacturer's or trade names does not constitute an official endorsement or approval of the use thereof.

Destroy this report when it is no longer needed. Do not return it to the originator.

Army Research Laboratory

Aberdeen Proving Ground, MD 21005

ARL-TR-6743 **December 2013**

Enhancing the High Temperature Capability of Nanocrystalline Alloys: Utilizing Thermodynamic Stability Maps to Mitigate Grain Growth Through Solute Selection

Mark A. Tschopp and Kristopher A. Darling

Weapons and Materials Research Directorate

Mark A. Atwater

Applied Engineering, Safety & Technology Department

Millersville University

Brian K. VanLeeuwen and Zi-Kui Liu

Department of Materials Science and Engineering

Pennsylvania State University

REPORT DOCUMENTATION PAGE

Form Approved
OMB No. 0704-0188

1. REPORT DATE *(DD-MM-YYYY)*	2. REPORT TYPE	3. DATES COVERED (From - To)
December 2013	Final	October 2012–December 2013

4. TITLE AND SUBTITLE
Enhancing the High Temperature Capability of Nanocrystalline Alloys: Utilizing Thermodynamic Stability Maps to Mitigate Grain Growth Through Solute Selection

5a. CONTRACT NUMBER

5b. GRANT NUMBER

5c. PROGRAM ELEMENT NUMBER

6. AUTHOR(S)
Mark A. Tschopp, Kristopher A. Darling, Mark Atwater[1], Brian K. VanLeeuwen[2], and Zi-Kui Liu[2]

5d. PROJECT NUMBER

5e. TASK NUMBER

5f. WORK UNIT NUMBER

7. PERFORMING ORGANIZATION NAME(S) AND ADDRESS(ES)
U.S. Army Research Laboratory
ATTN: RDRL-WMM-F
Aberdeen Proving Ground, MD 21005

8. PERFORMING ORGANIZATION REPORT NUMBER
ARL-TR-6743

9. SPONSORING/MONITORING AGENCY NAME(S) AND ADDRESS(ES)

10. SPONSOR/MONITOR'S ACRONYM(S)

11. SPONSOR/MONITOR'S REPORT NUMBER(S)

12. DISTRIBUTION/AVAILABILITY STATEMENT
Approved for public release; distribution is unlimited.

13. SUPPLEMENTARY NOTES
[1] Applied Engineering, Safety & Technology Department, Millersville University
[2] Department of Materials Science and Engineering, Pennsylvania State University

14. ABSTRACT
Mitigating grain growth at high temperatures in binary nanocrystalline alloys is important for processing nanocrystalline alloy systems. The objective of this research is to develop a methodical design-based approach for selecting solutes in binary nanocrystalline alloys by revisiting grain boundary thermodynamics and the internal processes of grain growth and solute segregation in a closed system. In this work, the grain boundary energy is derived and systematically studied in terms of temperature, grain size, concentration, and solute segregation for binary systems of 44 solvents and 52 solutes, using readily-available elemental data, such as moduli and liquid enthalpy of mixing. It is shown that through solute segregation, the grain boundary energies of some binary systems can be reduced, resulting in thermodynamically stable grain structures and successful prediction of solutes that inhibit grain growth in some nanocrystalline alloys. Parametric studies reveal trends between equilibrium grain size, solute distribution and temperature for various binary systems culminating in the generation of nanocrystalline thermodynamic stability maps as a tool for solute selection in binary nanocrystalline alloys.

15. SUBJECT TERMS
nanocrystalline materials, grain growth, grain boundary energy, grain boundary segregation

16. SECURITY CLASSIFICATION OF:			17. LIMITATION OF ABSTRACT	18. NUMBER OF PAGES	19a. NAME OF RESPONSIBLE PERSON
a. REPORT	b. ABSTRACT	c. THIS PAGE			Mark A. Tschopp
Unclassified	Unclassified	Unclassified	UU	46	19b. TELEPHONE NUMBER (*Include area code*) 410-306-0855

Standard Form 298 (Rev. 8/98)
Prescribed by ANSI Std. Z39.18

Contents

List of Figures iv

List of Tables v

Acknowledgments vi

1. Introduction 1

2. Thermodynamics of Grain Growth and Segregation 2

3. Application to Grain Size Stabilization in Fe–Zr and Other Binary Systems 6

3.1 Grain Boundary Stabilization in the Fe–Zr System 6

3.2 Grain Boundary Stabilization in Other Binary Systems 14

3.3 Thermodynamic Stability Map Changes with Temperature 32

3.4 Relationship between Solute Concentrations 36

4. Summary and Conclusions 40

5. References 41

Distribution List 44

List of Figures

Figure 1. Bilayer grain boundary used for the regular solution model. 9

Figure 2. Grain boundary energy γ/γ_0 vs. mol fraction of Zr atoms. 10

Figure 3. Stabilized grain size and inverse grain size as a function of temperature for various Zr content. 11

Figure 4. Stabilized grain size vs. temperature for various ΔH_{mix}. 12

Figure 5. Nanocrystalline Fe stability map. 20

Figure 6. Nanocrystalline Ni stability map. 21

Figure 7. Nanocrystalline Cu stability map. 22

Figure 8. Nanocrystalline Al stability map. 23

Figure 9. Nanocrystalline Mg stability map. 24

Figure 10. Nanocrystalline Ti stability map. 25

Figure 11. Nanocrystalline Pd stability map. 26

Figure 12. Nanocrystalline W stability map. 27

Figure 13. Nanocrystalline Fe stability map for various temperatures. 33

Figure 14. Nanocrystalline stability map for various elements ($T = 0.3T_m$). 34

Figure 15. Nanocrystalline stability map for various elements ($T = 0.8T_m$). 35

Figure 16. Grain boundary solute and interior concentration plots. 38

Figure 17. Grain boundary solute to interior concentration for various grain sizes. 39

List of Tables

Table 1. Parameters of the Fe–Zr binary system.. 13

Table 2. Solutes and concentrations for nanocrystalline Fe. 17

Table 3. Solutes and concentrations for nanocrystalline Ni. 18

Table 4. Solutes and concentrations for nanocrystalline Cu. 19

Table 5. Solutes and concentrations for nanocrystalline Al. 28

Table 6. Solutes and concentrations for nanocrystalline Mg. 29

Table 7. Solutes and concentrations for nanocrystalline Ti. 30

Table 8. Solutes and concentrations for nanocrystalline Pd. 30

Table 9. Solutes and concentrations for nanocrystalline W. 31

Acknowledgments

This work is supported in part by the U.S. Army Research Laboratory (ARL) under contract GS04T09DBC0017. Dr. Mark Tschopp would like to acknowledge partial support from ARL administered by the Oak Ridge Institute for Science and Education through an interagency agreement between the U.S. Department of Energy and ARL (October 2012–September 2013). Dr. Mark Tschopp would like to acknowledge continued support for this work from ARL through the High Performance Technology Group at Dynamic Research Corporation under the Special Project "Atomistic Modeling Development for Nanocrystalline Metal Alloys" (October 2013–December 2013). Dr. Zi-Kui Liu would like to acknowledge support from the National Science Foundation under grant DMR-1005677.

1. Introduction

For nanocrystalline materials to be useful, they must be sufficiently resistant to grain growth at elevated temperatures to retain their nanoscale grain size ($d < 100\,\text{nm}$). One strategy for stabilizing nanocrystalline materials is to add segregating solutes to reduce the grain boundary energy (*1–11*). Since grain boundary energy is the driving force for grain growth, a reduction in grain boundary energy can impede or even entirely inhibit grain growth. The reduction in grain boundary energy provided by a segregating solute is determined by the segregation energy, ΔG_{seg} (*1–11*). Since the values of ΔG_{seg} are usually not available, they are estimated. Wynblatt and Chatain (*12*) recently reviewed the analytical models on segregation to grain boundaries (GBs) and surfaces and addressed the difficulty of meaningful definitions of segregation enthalpy, entropy, and free energy among various issues. The central equation for all models is as follows for a binary system:

$$\frac{x_B^{GB}}{1-x_B^{GB}} = \frac{x_B^I}{1-x_B^I}\text{exp}\left[-\frac{\Delta G_{seg}^{ex}}{RT}\right], \tag{1}$$

where x_B^{GB} and x_B^I are the mole fractions of component B (solute) in the grain boundary and grain interior, respectively, ΔG_{seg}^{ex} is the excess Gibbs energy of segregation, and R and T are the gas constant and absolute temperature, respectively. The Gibbs energy of segregation is thus defined as follows:

$$\Delta G_{seg} = \Delta H_{seg} - T\Delta S_{seg} = \left(\Delta H_{seg} - T\Delta S_{seg}^{ex}\right) - T\Delta S_{seg}^{ideal} = \Delta G_{seg}^{ex} - T\Delta S_{seg}^{ideal}, \tag{2}$$

where ΔH_{seg}, ΔS_{seg}, and ΔS_{seg}^{ideal} are the enthalpy, entropy and ideal entropy of segregation, respectively. Equation 1 is thus obtained by setting equation 2 equal to zero, i.e.,

$$\Delta G_{seg} = 0, \tag{3}$$

indicating zero driving force for solute segregation to the interface. With a given model for ΔG_{seg}^{ex} the compositions in the grain boundary and grain interior can be obtained and are further

used to evaluate the grain boundary energy of isotropic or anisotropic systems.

Conventionally, the interfacial energy is defined as the reversible work needed to create a unit area of surface (e.g., grain boundary) at constant temperature, volume (or pressure), and chemical potentials, i.e., for an open system (*12*). However, in practical applications, the interfacial energy is measured in a closed system (i.e., constant compositions). In the present work, we will first derive the expression of grain boundary energy for a closed system by differentiating the internal and external variables and defining the internal processes, and then predict the effect of segregating solutes on the grain boundary energy in binary systems of 44 solvents and 52 solutes. This reduction in grain boundary energy will be used to select nanocrystalline alloys in terms of thermal stability.

2. Thermodynamics of Grain Growth and Segregation

The combined first and second law of thermodynamics of a system can be written as (*13*)

$$dG = -SdT + VdP + \sum_i \mu_i dN_i - Dd\xi, \tag{4}$$

where G, S, V, and μ_i are the Gibbs energy, entropy, volume, and chemical potential of component i of the system; T, P, and N_i are temperature, pressure, and moles of component i controlled from surroundings; ξ and D represent the extent of an internal process and its driving force and more than one simultaneous internal processes can be considered as shown below. For a system with a grain boundary area of A which reaches a metastable equilibrium under constant temperature, pressure, and compositions, each term in equation 4 becomes zero, i.e.,

$$dG = 0, \tag{5}$$

Let us now consider an internal process with the grain boundary area changed by dA. Due to the composition difference between the grain boundary and the grain interior, there will be a simultaneous redistribution of elements, commonly referred to as segregation. These two internal processes contribute to the change of Gibbs energy of the system as follows (*13*):

$$dG = \sum_i \left(\mu_i^{GB} - \mu_i^I\right) dn_i + \gamma_0 dA, \tag{6}$$

where μ_i^{GB} and μ_i^I are the chemical potentials of component i in the grain boundary and grain interior, respectively, dn_i is the change of component i from the grain interior to the grain boundary, and γ_0 is the change in G due to a change in A at constant n_i, i.e.,

$$\gamma_0 = \left(\frac{\partial G}{\partial A}\right)_{n_i,T,P,N_i}. \tag{7}$$

$\mu_i^{GB} - \mu_i^I$ can be further written as

$$\mu_i^{GB} - \mu_i^I = RT\ln\left(\frac{x_i^{GB}}{x_i^I}\right) + G_i^{ex/GB} - G_i^{ex/I}, \tag{8}$$

where $G_i^{ex/GB}$ and $G_i^{ex/I}$ are the partial excess Gibbs energy of component i in the grain boundary and grain interior, respectively. For a binary A-B system, we have $dn_A = -dn_B$, and equation 6 can be rewritten as

$$dG = \left[RT\ln\left(\frac{x_B^{GB}}{1-x_B^{GB}}\frac{1-x_B^I}{x_B^I}\right) + \Delta G_{seg}^{ex}\right] dn_B + \gamma_0 dA = \Delta G_{seg} dn_B + \gamma_0 dA, \tag{9}$$

where ΔG_{seg}^{ex} and ΔG_{seg} are defined as

$$\Delta G_{seg}^{ex} = G_B^{ex/GB} - G_B^{ex/I} - \left(G_A^{ex/GB} - G_A^{ex/I}\right) = G_B^{ex/GB} - G_A^{ex/GB} - \left(G_B^{ex/I} - G_A^{ex/I}\right), \tag{10}$$

and

$$\Delta G_{seg} = \left(\frac{\partial G}{\partial n_B}\right)_{A,T,P,N_A,N_B}, \tag{11}$$

It is evident from the above equations that the grain boundary energy for a closed system is defined as (*14*)

$$\gamma = \left(\frac{\partial G}{\partial A}\right)_{T,P,N_A,N_B} = \Delta G_{seg}\frac{\partial n_B}{\partial A} + \gamma_0, \tag{12}$$

There are two significant observations from the above derivations: (1) ΔG^{ex}_{seg} is related to the partial quantities of excess Gibbs energy of grain and grain boundary, not the excess Gibbs energies themselves, and (2) $\gamma = \gamma_0$ when $\Delta G_{seg} = 0$, i.e., equation 3 and equation 1, meaning there is no redistribution of elements during a change of grain boundary area. The latter is a constrained equilibrium, because it poses a limitation on an internal process for a closed system, which would otherwise take place to reduce the Gibbs energy of the system. Therefore, the widely used equation 1, commonly referred to as Langmuir–McLean (or Fowler–Guggenheim) segregation isotherm is applicable when the redistribution of elements is negligible during measurements of grain boundary energies. If this is not the case, equation 12 should be used for grain boundary energy.

There are many models on how to treat ΔH_{seg} and ΔS^{ex}_{seg} in equation 2 as discussed by Wynblatt and Chatain (*12*) including their dependences on five degrees of freedom of grain boundaries. As the purpose of this work is to compare the effects of a wide range of alloying elements, we follow the Wynblatt and Ku model for surface segregation (*12, 15*) and assume $\Delta S^{ex}_{seg} = 0$. Therefore,

$$\Delta H_{seg} = \Delta H^{chem}_{seg} + \Delta H^{elastic}_{seg}, \tag{13}$$

where

$$\begin{aligned}\Delta H^{chem}_{seg} = &\left(\gamma_B\sigma_B - \gamma_A\sigma_A\right)(1-\alpha) \\ &- \frac{2\Omega}{z}\left[z_l\left(x^{GB}_B - x^I_B\right) - z_v\left(x^I_B - \frac{1}{2}\right) + \alpha z_v\left(x^{GB}_B - \frac{1}{2}\right)\right],\end{aligned} \tag{14}$$

and

$$\Delta H^{elastic}_{seg} = \frac{-24\pi N_{Av}K_B G_A r_A r_B\left(r_B - r_A\right)^2}{3K_B r_A + 4G_A r_B}. \tag{15}$$

In the above equations, γ_A, γ_B, σ_A, and σ_B are the free surface energies and the grain boundary areas per mole of grain boundary atoms of components A (solvent) and B (solute), respectively.

α is a bond energy interaction parameter introduced to distinguish the bond energy in the lattice region from the grain boundary region. If $\alpha = 0$, the expression is equivalent to the surface segregation model. Ω is the regular solution interaction parameter that can be approximated as four times the liquid enthalpy of mixing of an equimolar alloy of the solute and solvent, ΔH_{mix}. ΔH_{mix} can be obtained in the literature (*16, 17*). Values for the liquid enthalpy of mixing are chosen over those of the solid states, because such values would include elastic contributions, which are considered separately in the equation. z_l and z_v are the coordination numbers in and out of the grain boundary plane regions, and z is the coordination number ($z = z_l + 2z_v$). The equation for $\Delta H_{seg}^{elastic}$ is based on analyses by Friedel (*18*) and Eshelby (*19*) with N_{Av} being Avogadro's number, K_B being the bulk modulus of the component B, G_A the shear modulus of the component A, and r_A and r_B are the atomic radii of components A and B. Equation 13 correctly considers both the chemical contributions (equation 14) to the segregation enthalpy, as well as the elastic enthalpy (equation 15), as proposed by Wynblatt and Chatain (*12*) and Wynblatt and Ku (*15*). Recently, Saber et al. (*20*) applied a similar model augmented with the Trelewicz and Schuh (*8*) analytical approach to four binary systems: Fe–Zr, Cu–Nb, Cu–Zr, Ni–W. In contrast to Saber et al., the present model uses the concept of internal state variables to define the metastable state. Additionally, we apply the present model to a much larger collection of binary systems (> 1000) using published experimental and predicted values, which necessitated the development of thermodynamic stability maps to organize the information and to guide alloy selection/development. The developed maps allow the visualization of trends governing thermodynamic stability that are not obvious given analysis of only a few systems.

3. Application to Grain Size Stabilization in Fe–Zr and Other Binary Systems

3.1 Grain Boundary Stabilization in the Fe–Zr System

For a given system under constant temperature, pressure and overall composition, the grain boundary energy represented by equation 12 is a function of x_B^{GB} and x_B^I, which are related by mass balance based on the grain size d and the grain boundary model. The Fe–Zr system is used to demonstrate the procedure. An experimental investigation for the stabilization of nanocrystalline Fe by additions of Zr solute was reported in (*10*). For bcc Fe with $\{110\}$ grain boundary planes, $z_l = 4$ and $z_v = 2$, and $\alpha = 5/6$. It is assumed that $\sigma_A = \sigma_B = \sigma = \sigma_{Fe} = N_{Av} V_{Fe}^{2/3}$ where V_{Fe} is the atomic volume of Fe (solvent).

For a bilayer grain boundary model shown schematically in figure 1, one can make the following approximation:

$$\Gamma = \frac{\partial n_B}{\partial A} = \frac{2\left(x_{Zr}^{GB} - x_{Zr}^{I}\right)}{\sigma}, \tag{16}$$

where Γ is the GB solute excess. With d being the volume-averaged grain size, the mass conservation in a closed system with a mole fraction x_0 of Zr added to Fe is

$$x_0 = \frac{2V_m\left(x_{Zr}^{GB} - x_{Zr}^{I}\right)}{\sigma}\frac{3}{d} + x_{Zr}^{I}, \tag{17}$$

where $3/d$ represents the grain boundary area per unit volume for the spherical grain shape, and V_m is the molar volume for the solvent Fe. Equation 12 can thus be rewritten in terms of the normalized grain boundary energy γ/γ_0,

$$\begin{aligned}\frac{\gamma}{\gamma_0} =& 1 + \frac{2\left(x_{Zr}^{GB} - x_{Zr}^{I}\right)}{\gamma_0\sigma}\left\{\frac{\gamma_{Zr} - \gamma_{Fe}}{6}\sigma - \right. \\ & \left. \Delta H_{mix}\left[\frac{17}{3}x_{Zr}^{GB} - 6x_{Zr}^{I} + \frac{1}{6}\right] + \Delta H_{seg}^{elastic} - RT\ln\left[\frac{x_{Zr}^{I}\left(1 - x_{Zr}^{GB}\right)}{\left(1 - x_{Zr}^{I}\right)x_{Zr}^{GB}}\right]\right\}.\end{aligned} \tag{18}$$

Figure 2 shows a typical plot of γ/γ_0 vs. x_{Zr}^{GB} for a range of grain size values at $x_0 = 0.03$ and $T = 550\,°\text{C}$ with other parameters given in table 1. It can be seen that each γ/γ_0 curve passes through a minimum for each grain size considered. The equilibrium condition of the system with respect to grain growth (*6*) is stipulated by equation 5, which is equivalent to setting equation 18 equal to zero, i.e., $\gamma/\gamma_0 = 0$. Figure 2 shows that the curve with $d = 23.1\,\text{nm}$ (filled red circles) has a minimum at $x_{Zr}^{GB} = 0.26$ with $\gamma/\gamma_0 = 0$. This grain size value is designated as d_m. For systems with $d < d_m$, there will be a thermodynamic driving force for grain growth to reduce the grain boundary area until $d = d_m$. For systems with $d > d_m$, there are two x_{Zr}^{GB} values where $\gamma/\gamma_0 = 0$ as shown in figure 2. However, it is evident that if these two states were put together, atomic diffusion would take place due to the different values of x_{Zr}^{GB} and x_{Zr}^{I} of the two states until both x_{Zr}^{GB} and x_{Zr}^{I} become homogeneous in grain boundary and grain interior, respectively, and the grain size adjusts itself to d_m based on the model.

Figure 3(a) shows the d_m grain size values as a function of temperature for a range of x_0 alloy contents. At higher solute concentrations x_0, there is additional solute to stabilize the grain boundaries. At the higher Zr contents, stabilization at a nanoscale grain size smaller than $100\,\text{nm}$ would be effective up to temperatures from $800\,°\text{C}$ to $900\,°\text{C}$. There is an abrupt destabilization as temperature increases above a limit, though. An alternative plot of the data in figure 3(a) is given in figure 3(b) where $1/d_m$ is plotted as a function of T and x_0. Complete loss of stabilization is revealed as these curves approach the $d_m \to \infty$ limit. Using a regular solution model in the limit of small x_0 values and fully saturated grain boundaries, Kirchheim (*6*) suggested that inverse grain size vs. $\ln T$ curves would be linear with a negative slope, in qualitative agreement with the plot in figure 3(a).

The grain boundary thermodynamic stabilization model used in the present work includes elastic size misfit energy, $\Delta H_{seg}^{elastic}$, and chemical bond energy ΔH_{seg}^{chem}. ΔH_{seg}^{chem} is manifested by the enthalpy of mixing, ΔH_{mix}, of an equimolar Fe–Zr liquid phase through the bond energy interaction parameter, α; however, the ΔH_{seg}^{chem} is dominated by the magnitude of the enthalpy of mixing ΔH_{mix}. $\Delta H_{seg}^{elastic}$ always favors grain boundary segregation. $\Delta H_{mix} > 0$ (demixing) favors grain boundary segregation whereas $\Delta H_{mix} < 0$ (mixing) favors grain boundary desegregation. The combination of these two contributions ($\Delta H_{mix} \propto \Delta H_{seg}^{chem}$ and $\Delta H_{seg}^{elastic}$) dictates the effect of an alloying element on grain boundary energy. The effect of ΔH_{mix} for Fe–Zr alloys is examined in figure 4 for $x_0 = 0.04$ by systematically changing the ΔH_{mix} values. For a hypothetical case of no chemical effect with $\Delta H_{mix} = 0$, $d_m = 10\,\text{nm}$ is predicted at the melting point of Fe. In an Fe–4%Zr alloy annealed at $913\,°\text{C}$, transmission electron microscopy and ion channeling contrast images indicated a volume average grain size of 57 ± 15 nm (*9*). In addition, x-ray diffraction data on the same alloy as a function of annealing temperature are

provided and plotted as blue stars in figures 3 and 4. A value of $\Delta H_{mix} = -24\,\mathrm{kJ\,mol^{-1}}$ is in excellent agreement with these experimental results and is pretty close to the $-25\,\mathrm{kJ\,mol^{-1}}$ obtained from the literature (see table 1). It is notable that the trends observed for the Fe–Zr results in reference (*10*) lend support to quantitative predictions for thermodynamic stabilization.

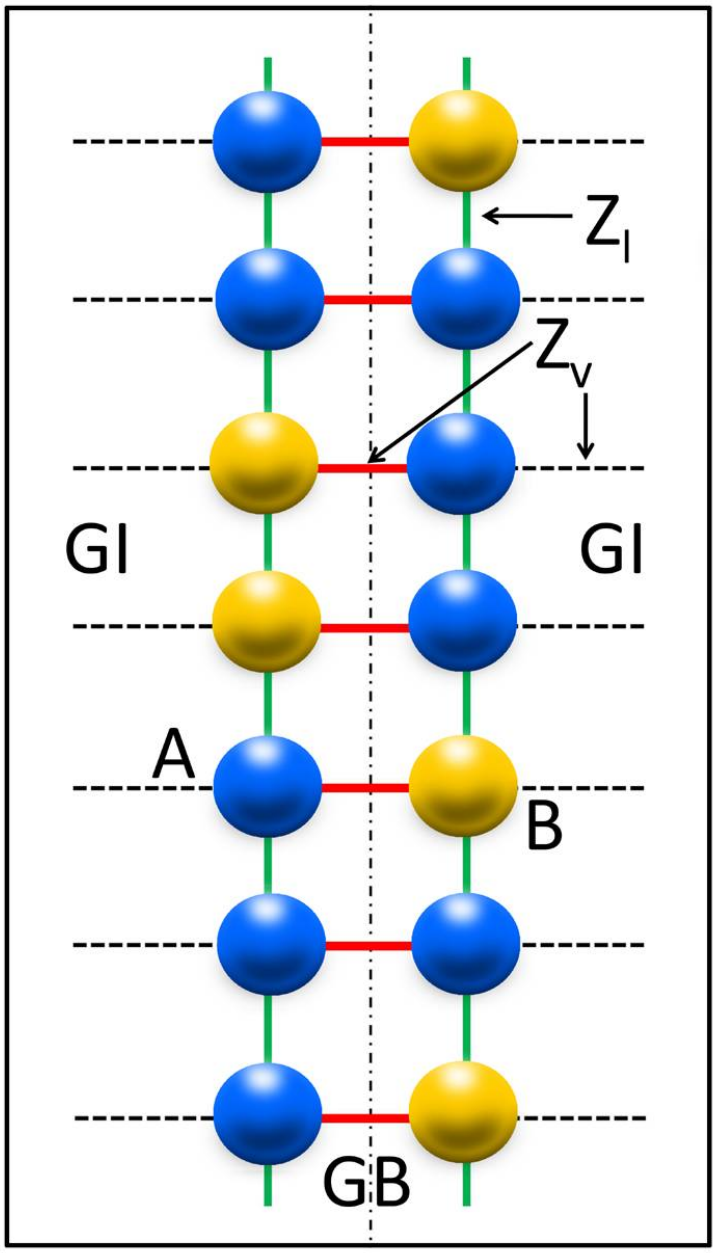

Figure 1. Bilayer grain boundary used for the regular solution model. z_l indicates in-plane bonds, and z_v indicates out-of-plane bonds. The latter can be bonds joining atoms across the grain boundary (GB) or bonds joining atoms on the GB to the grain interior (GI). Solvent (A) and solute (B) atoms are shown on the GB bilayers.

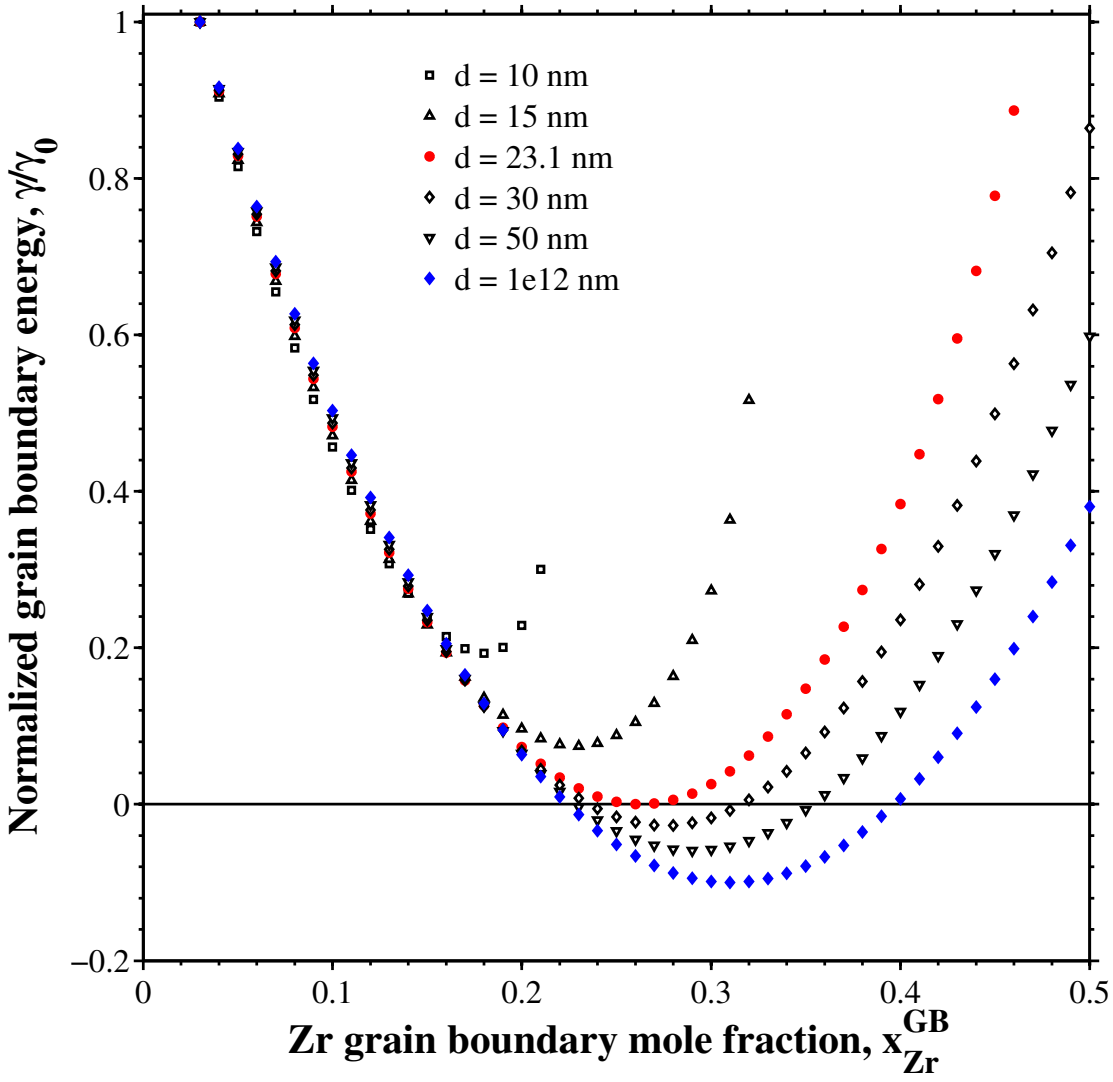

Figure 2. Normalized grain boundary energy γ/γ_0 vs. mol fraction of Zr atoms on the grain boundary for several different grain sizes: 10, 15, 23.1, 30, 50 and 1×10^{12} nm. The molar Zr fraction x_0 is 0.03 and the temperature T is 550 °C for this plot. The plot intersects $\gamma/\gamma_0 = 0$ at a grain size of 23.1 nm, which corresponds to the stabilized grain size, d_m.

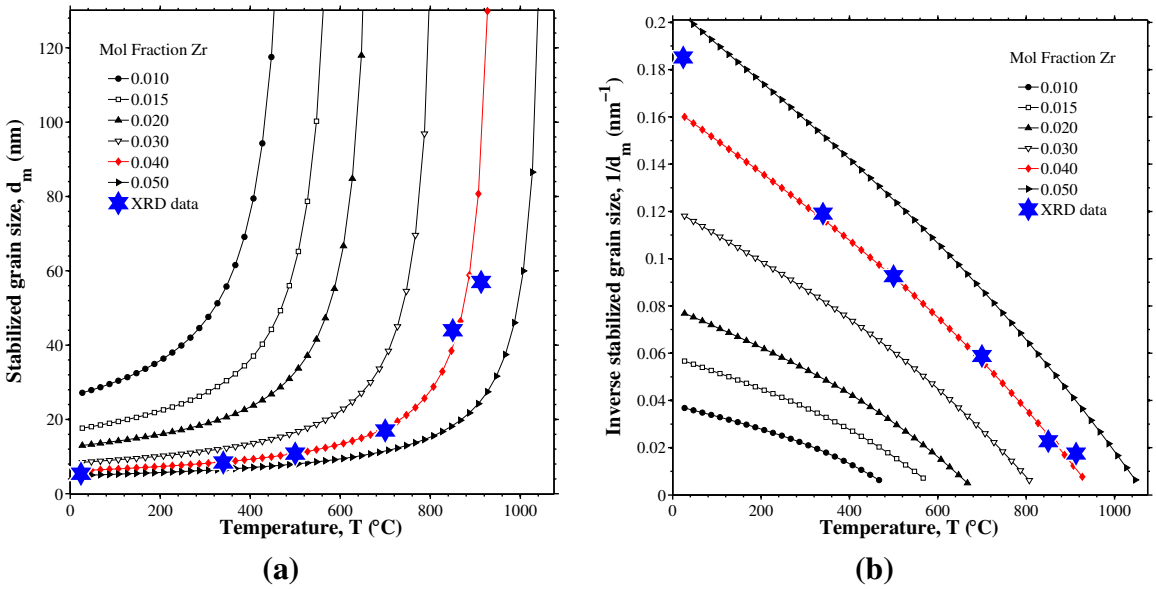

Figure 3. (a) Stabilized grain size d_m and (b) inverse grain size as a function of temperature T for different Zr molar fractions, x_0: 0.01, 0.015, 0.02, 0.03, 0.04 and 0.05. Experimental X-ray diffraction (XRD) and transmission electron microscopy (TEM) data for an Fe–4%Zr alloy are plotted as blue stars (*9, 10*). ΔH_{mix} of -24 kJ mol^{-1} is used to show agreement with the experimental XRD/TEM data. The inverse grain size shows a linear dependence on temperature T with some deviation from linearity at lower temperatures.

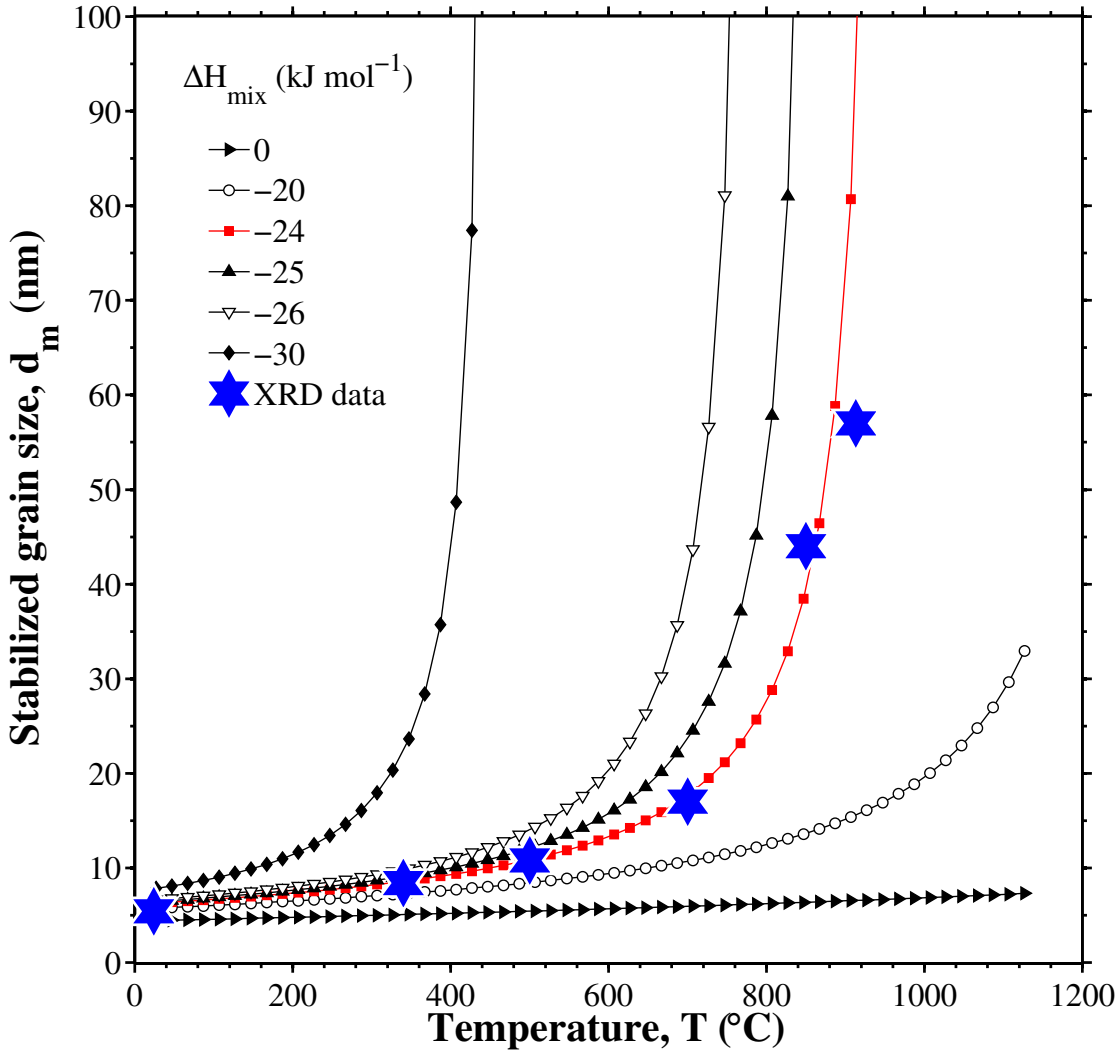

Figure 4. Stabilized grain size d_m vs. temperature T for molar Zr fraction $x_0 = 0.04$ and different ΔH_{mix} values: 0, -20, -24, -25, -26 and -30 kJ mol^{-1}. Experimental XRD and TEM data for an Fe–4%Zr alloy are plotted as blue stars (*9, 10*). $\Delta H_{mix} = -24$ kJ mol^{-1} shows excellent agreement with the experimental XRD/TEM data.

Table 1. Parameters of the Fe–Zr binary system.

Property	Value/Units	Equation or Reference
α	$5/6$	$\alpha = \epsilon_{intergranular}/\epsilon_{intragranular}$
z	8	BCC, $z = z_l + 2z_v$
z_v	2	BCC, $\{110\}$
z_l	4	BCC, $\{110\}$
γ_0	$0.795\,\mathrm{J\,m^{-2}}$	Ref. (*21, 22*)
γ_{Zr}	$1.909\,\mathrm{J\,m^{-2}}$	Ref. (*21, 22*)
γ_{Fe}	$2.417\,\mathrm{J\,m^{-2}}$	Ref. (*21, 22*)
K_{Zr}	$89.8\,\mathrm{GPa}$	Ref. (*23*)
G_{Fe}	$81.6\,\mathrm{GPa}$	Ref. (*23*)
V_{Fe}	$0.0118\,\mathrm{nm^3}$	Ref. (*23*)
V_{Zr}	$0.0233\,\mathrm{nm^3}$	Ref. (*23*)
ΔH_{mix}	$-25\,\mathrm{kJ\,mol^{-1}}$	Ref. (*16, 17*)
$\Delta H_{seg}^{elastic}$	$-108\,\mathrm{kJ\,mol^{-1}}$	Equation 16
σ	$31\,217\,\mathrm{m^2\,mol^{-1}}$	$N_{Av}V_{Fe}^{2/3}$
V_m	$7.107 \times 10^{-6}\,\mathrm{m^3\,mol^{-1}}$	$N_{Av}V_{Fe}$

3.2 Grain Boundary Stabilization in Other Binary Systems

The same approach is subsequently applied to other binary systems of 44 solvents each with 52 solutes. For instance, table 2 lists the solute concentrations required to thermally stabilize the binary system at a given grain size (25 nm) with a given solute for a particular solvent (in this case, Fe) at a given temperature ($0.60T_M^{Fe} \approx 1200$ K). For each solute (of 52), the following quantities were obtained for the solvent: the enthalpy of mixing ΔH_{mix}, the free surface energy γ_B, the bulk modulus K_B, the molar volume V_M^B, and atomic radii r_B. Some of these are required to calculate the elastic enthalpy term $\Delta H_{seg}^{elastic}$ using equation 15. Then, the content of each solute was changed from 0.1% to 10% in increments of 0.1% to find the minimum solute concentration required to stabilize the system, i.e., $\gamma/\gamma_0 = 0$ (equation 18). Table 2 represents all solutes and their minimum concentration x_0 required to stabilize the solvent Fe at a grain size of 25 nm for a temperature of $0.60T_M^{Fe}$. The elastic enthalpy $\Delta H_{seg}^{elastic}$ and enthalpy of mixing ΔH_{mix} are also included along with the grain boundary solute excess Γ for the bilayer model, which represent reasonable values. This table does not include those solutes that were not predicted to stabilize the system, $\gamma/\gamma_0 > 0$ for all $x_0 \leq 0.10\%$. For stabilization of a *larger* grain size at the *same* temperature, lower solute concentrations are required (e.g., for 100 nm, 4.8% Zr or 0.2% Ca). This would be expected, since there is a lower total grain boundary area at larger grain sizes. Similarly, for stabilization of the *same* grain size at a *lower* temperature, lower solute concentrations are again required. While there are a number of solutes that would not be selected due to their high price, toxicity, low melting temperature, etc., this model may shed light on prospective binary nanocrystalline systems from a thermodynamic stability standpoint. Additionally, some solutes may drive the interfacial energy down, but could be embrittle the grain boundary. Hence, this model is only one criteria of several that would be important for selecting nanocrystalline binary systems.

The solutes that are effective at stabilizing the nanocrystalline grain structure are functions of both the elastic enthalpy and the enthalpy of mixing. Figure 5 is a plot of the elastic enthalpy versus the enthalpy of mixing for both the stabilizing solutes (table 2) as well as the solutes that do not appear in table 2. The red and black dots denote the stabilizing and nonstabilizing solutes, and the size of the dot for the stabilizing solutes corresponds to the magnitude of the minimum solute concentration required to stabilize a grain size of 25 nm. Moreover, a convex hull* of all of the systems (dotted line), the stabilizing solutes (red line), and the nonstabilizing solutes (black line) is plotted to delineate the nanocrystalline stability design space. Interestingly, there is a noticeable division of the solutes that stabilize the nanocrystalline grain structure from those that don't. Therefore, figure 5 and similar plots can be envisioned as 'nanocrystalline stability maps.'

*In computational geometry, a convex hull for of a set X of points is the smallest convex set that contains X.

There are a few general trends that emerge from the nanocrystalline stability map (figure 5). The first general trend observed is that the larger the magnitude of the elastic enthalpy (i.e., more negative) of the solute, the smaller the bulk solute concentration required for stabilization. Additionally, the magnitude and sign of the enthalpy of mixing detract from or reinforce stabilization, with negative values tending to reduce stability in any given system. Furthermore, stabilized systems that require higher solute concentrations tend to have a lower driving force for segregating to the boundary. Of the nonstabilized systems, there were a number of systems that reduced the excess grain boundary free energy, but did not reduce it to zero (recall that $\gamma/\gamma_0 = 0$ is required for stabilized systems); in a very limited number of cases, bulk solute concentrations greater than 10% reduced the grain boundary energy to zero. However, in general, increasing the solute content even to moderately high levels (>5%) is not always a good practice as precipitate formation is exacerbated at higher solute contents and with increased temperature. Experimental observations generally show that secondary phases must be kinetically hindered (*24*) from forming, since they compete for the available solute, causing destabilization of the boundaries and rapid grain coarsening. Additionally, attention must be paid to the extent of forced solubility that can be attained by a given processing method, as this ultimately limits the amount of solute available for segregation to boundaries.

Using the above rational, tables for other solvents that are often associated with nanocrystalline materials are also presented. The other solvents are Ni, Cu, Al, Mg, Ti, Pd, and W (tables 3–9). Moreover, the same nanocrystalline stability maps are shown for the stabilizing solutes in these systems as well (figures 6–12). A few general themes are observed for these systems:

1. *In a number of systems, the majority of stabilizing solutes have a positive enthalpy of mixing.* For instance, the majority of stabilizing solutes in the Mg, Ti, Al, and W systems have a positive enthalpy of mixing. Currently the authors are unaware of any thermodynamic reports of grain growth prevention for nanocrystalline Mg, Ti, Al, or W. Additionally, it should be noted that many of the predicted stabilizing agents (e.g., Cs, Rb, K, Ba, Na, In, Sn, Tl, Sb and Pb), have been suggested by Seah to be grain boundary embrittling agents (*25*). Interestingly, in Ti, all of the stabilizing solutes have a positive enthalpy of mixing and there is a clear delineation between the stabilizing and nonstabilizing solutes. In the W system, a large variety of possible stabilizing solutes exist with the majority of the systems requiring a larger bulk solute content than many of the other systems examined. Additionally, due to the high melting point of W, high temperature stability will suffer from intermetallic formation at much lower temperatures.

2. *A positive enthalpy of mixing is not necessarily required for nanocrystalline stability.* For

instance, in the Ni- and Cu-based stabilized systems, an equal number of positive and negative enthalpy of mixing systems are indicated over the given range. Even for Fe, Al, Mg, W, there are several stabilizing solutes with negative enthalpies of mixing. However, the stabilizing solutes all tend to have a greater magnitude of elastic enthalpy in these cases to balance out the negative enthalpy of mixing. On the other hand, the majority of the nonstabilized systems have a negative enthalpy of mixing values and tend to form intermetallics. This is as expected, since negative enthalpy of mixing values lower the segregation enthalpy and the system orders resulting in oscillations of the composition; for positive enthalpy of mixing values, segregation is enhanced by forming clusters and/or by multilayer segregation (*26*).

3. *The limited experimental data supports the grouping of stabilizing and nonstabilizing solutes from the nanocrystalline stability maps.* Experimentally, there are few studied systems for either Ni or Cu, for which the grain growth was classified as being controlled thermodynamically. While a lack of grain growth was observed for nanocrystalline Ni–W and it is reasoned to be thermodynamic in nature, estimates by Schuh et al. suggested only a 60% reduction in excess grain boundary energy was possible, and thus true equilibrium was not met (*4*). Large reductions in grain boundary energy were calculated for W solute in Ni with the present model ($\approx$40%–60% at high solute concentration $>$10%); since true thermodynamic equilibrium was not reached, W is not suggested to be a true stabilizing agent for Ni (table 3). Additionally, Cu has been experimentally added to nanocrystalline Ni and has shown minor improvements in delaying the onset of grain growth at $T < 0.33T_m$ (*27*); however, in agreement with our stability maps, Cu is not listed as a stabilizing solute for annealing temperatures $T < 0.50T_m$.

   There have been a few studies which examined thermodynamically stabilizing nanocrystalline Cu with elements such as Ta and Zr, which are both listed as potential candidates (table 4). Recent atomic simulations on Ta dissolved in nanocrystalline Cu have shown that in the segregated state, Ta can prevent grain growth even at high homologous temperatures $>0.70T_M^{Cu}$ (*28*). Zr additions to Cu have shown mixed support of thermodynamic stability; the delineation between kinetic and thermodynamic modes of stability were unclear (*29*). The data in table 4 indicates a high Zr concentration needed for stabilization. Interestingly, based on experimental results of several binary systems presented in the nanocrystalline stability maps, most binary systems that are effective at grain stabilization tend to lie at the boundary of the convex hull for stabilizing solutes (Fe–Zr, Cu–Nb), and these are close to those solutes that are not predicted to be effective grain stabilizers. On the other hand, those systems that have not been effective at grain

stabilization (Cu–Zr) tend to lie on the interior of the convex hull.

4. *In some systems, most solutes tend to have a negative enthalpy of mixing, thus limiting the thermodynamic stability of the nanocrystalline grain structure.* For example, in the Pd system, there is only one solute (Bi) that can stabilize the grain size. However, it is well known that Bi acts as an embrittlement agent at grain boundaries. Since most solutes for Pd have only negative enthalpies of mixing, this may help explain the lack of stabilizing solutes in this nanocrystalline system.

Table 2. Solutes and their concentrations that stabilize the grain structure in nanocrystalline Fe at temperature $T = 0.60T_M^{Fe} = 921\,^{\circ}\mathrm{C}$ (1194 K) and grain size $d_m = 25$ nm.

System (Fe–X)	$\Delta H_{seg}^{elastic}$ (kJ mol^{-1})	ΔH_{mix} (kJ mol^{-1})	x_0 (at%)	Γ (μmol m^{-2})
Th	-187	-11	0.6	6.4
Ca	-143	25	0.7	7.6
Pb	-135	29	0.7	7.6
Bi	-135	26	0.7	7.6
Sr	-123	34	0.8	8.7
Y	-149	-1	0.8	8.5
Ba	-120	37	0.8	8.7
La	-138	5	0.8	8.5
K	-50	81	0.9	9.9
Rb	-53	83	0.9	9.9
Sn	-123	11	0.9	9.5
Sb	-124	10	0.9	9.5
Cs	-46	85	0.9	9.9
Tl	-77	31	1.1	11.7
Na	-36	62	1.2	13.1
In	-73	19	1.4	14.4
Mg	-52	18	1.9	19.1
Hg	-45	22	1.9	19.5
Ag	-31	28	2.0	20.8
Cd	-47	17	2.1	21.0
Li	-14	26	2.5	26.0
Sc	-95	-11	2.7	18.4
Au	-39	8	4.4	30.9
Hf	-106	-21	5.0	17.1
Zr	-109	-25	5.8	16.1

Table 3. Solutes and their concentrations that stabilize the grain structure in nanocrystalline Ni at temperature $T = 0.60T_M^{Ni} = 872\,^{\circ}\mathrm{C}$ (1145 K) and grain size $d_m = 25$ nm.

System (Ni–X)	ΔH_{el} (kJ mol^{-1})	ΔH_{mix} (kJ mol^{-1})	x_0 (at%)	Γ (μmol m^{-2})
Th	-202	-39	0.6	6.9
Ca	-149	-7	0.7	8.0
Pb	-148	13	0.7	8.2
Bi	-145	10	0.7	8.1
Y	-161	-31	0.8	8.8
Sn	-137	-4	0.8	9.0
Sb	-136	-1	0.8	9.0
Sr	-128	-1	0.9	10.1
Ba	-124	0	0.9	10.1
La	-147	-27	1.0	10.5
K	-51	45	1.1	12.7
Rb	-54	47	1.1	12.8
Cs	-46	48	1.1	12.7
Tl	-85	13	1.2	13.2
Na	-38	32	1.5	17.0
In	-82	2	1.7	17.4
Ag	-41	15	2.4	25.6
Hg	-51	8	2.5	25.0
Au	-52	7	2.9	28.0
Cd	-55	2	3.4	28.1
Mg	-60	-4	6.1	27.4

Table 4. Solutes and their concentrations that stabilize the grain structure in nanocrystalline Cu at temperature $T = 0.60T_M^{Cu} = 650\,^{\circ}\mathrm{C}$ (923 K) and grain size $d_m = 25$ nm.

System (Cu–X)	$\Delta H_{seg}^{elastic}$ (kJ mol^{-1})	ΔH_{mix} (kJ mol^{-1})	x_0 (at%)	Γ (μmol m^{-2})
Th	-169	-24	0.5	5.4
Ca	-139	-13	0.6	6.4
Pb	-123	15	0.6	6.5
Bi	-127	15	0.6	6.6
Y	-137	-22	0.7	7.3
Sb	-114	7	0.7	7.5
Sr	-121	-9	0.8	8.4
Sn	-109	7	0.8	8.5
Ba	-118	-9	0.8	8.3
La	-131	-21	0.8	8.2
Rb	-53	27	1.1	11.7
Tl	-72	15	1.1	11.5
K	-50	25	1.2	12.7
Cs	-46	28	1.2	12.7
In	-67	10	1.3	13.2
Na	-36	16	1.9	19.4
Hg	-42	8	2.3	21.9
W	-20	22	2.5	26.1
Cd	-42	6	2.7	24.6
Mo	-18	19	2.8	29.0
Re	-14	18	3.4	31.6
Hf	-85	-17	4.6	16.3
Zr	-91	-23	6.0	14.8
Mg	-47	-3	6.8	26.3
U	-62	-7	7.0	22.2
Nb	-40	3	7.2	29.0
Ta	-44	2	8.4	28.2

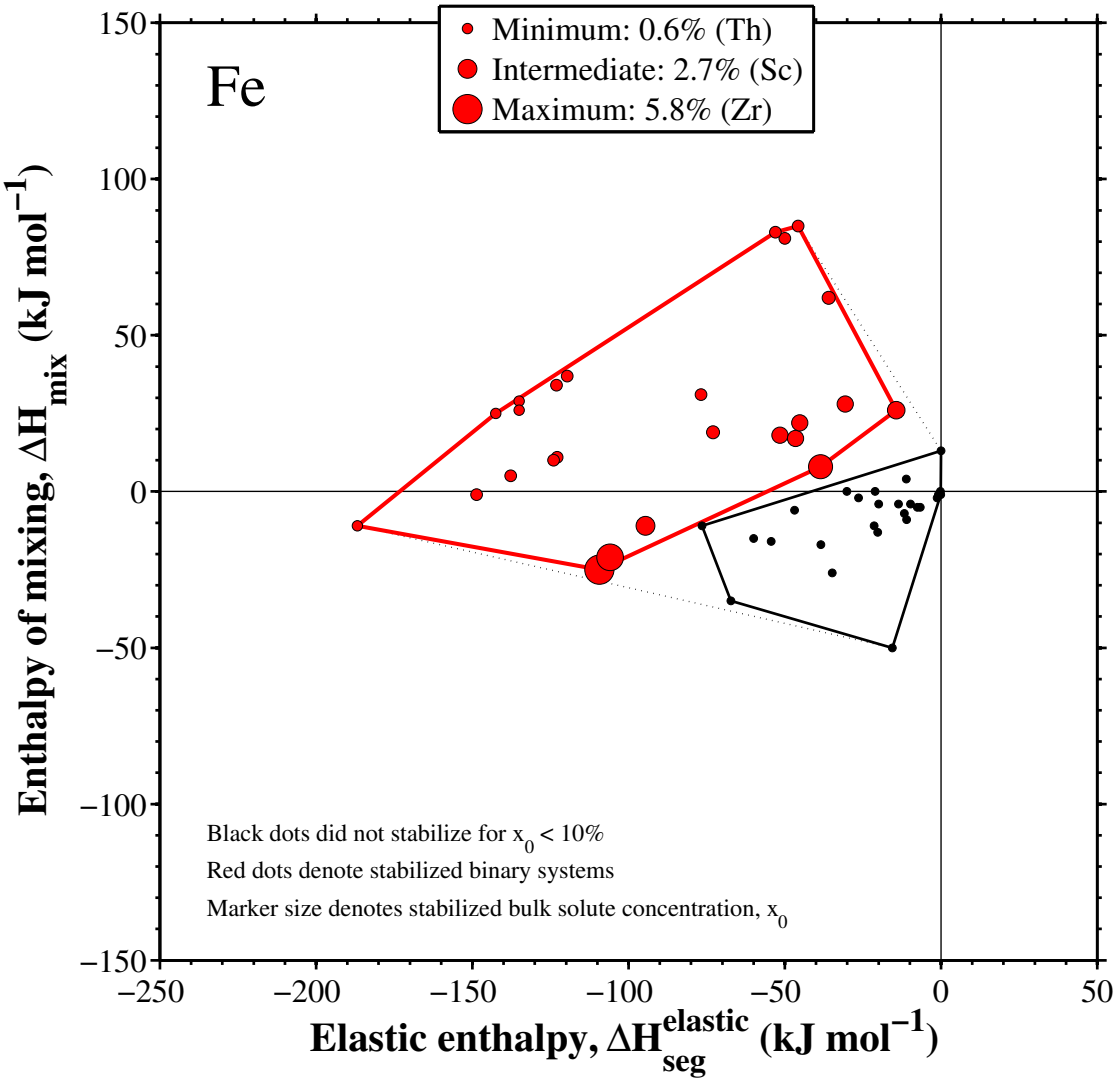

Figure 5. Nanocrystalline Fe stability map that plots the elastic enthalpy versus the enthalpy of mixing for both the stabilizing solutes (table 2, plotted as red dots) as well as the solutes that do not appear in table 2, plotted as black dots. The size of the dot for the stabilizing solutes corresponds to the magnitude of the minimum solute concentration required to stabilize a grain size of 25 nm.

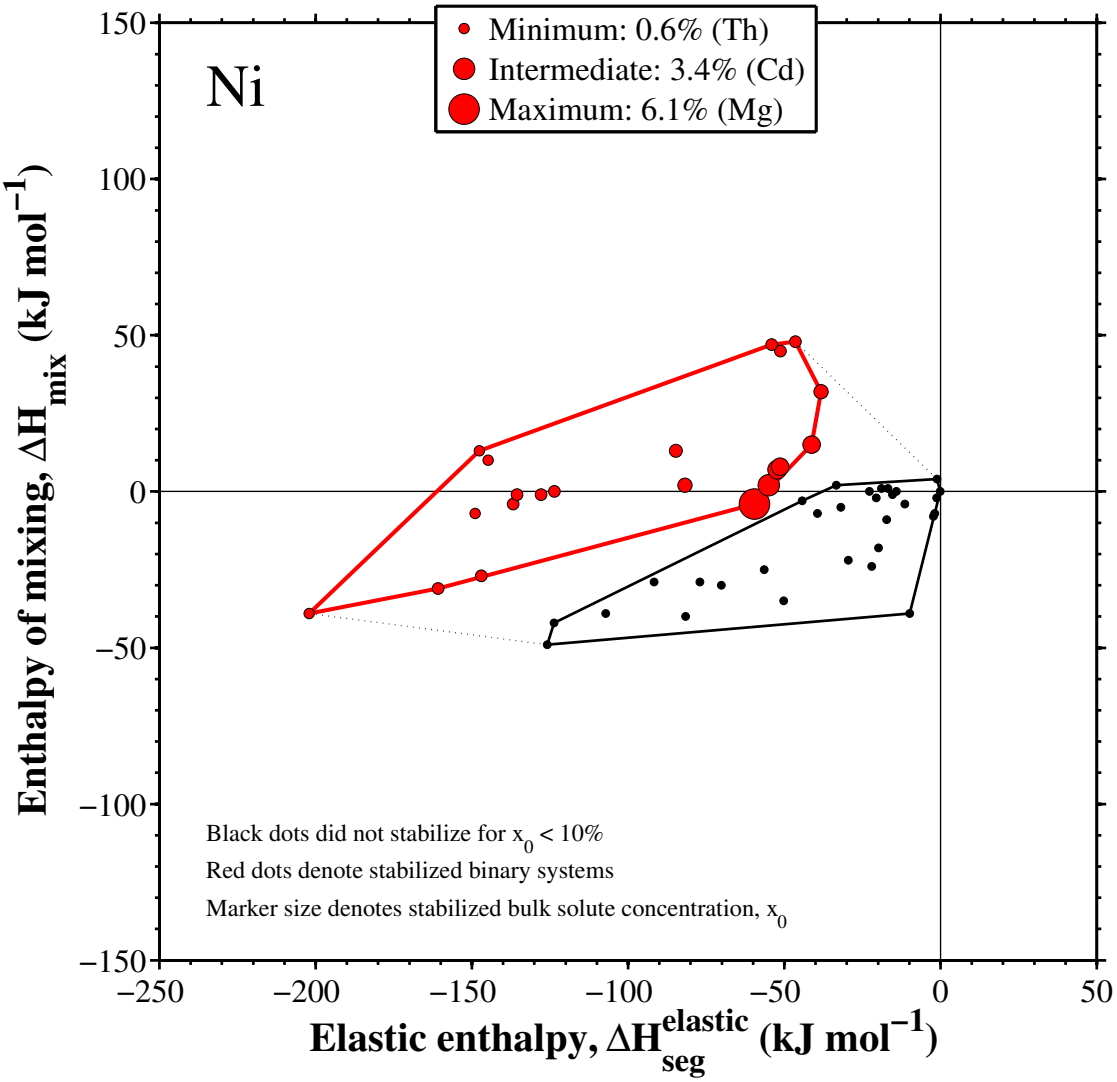

Figure 6. Nanocrystalline Ni stability map that plots the elastic enthalpy versus the enthalpy of mixing for both the stabilizing solutes (table 3, plotted as red dots) as well as the solutes that do not appear in table 3, plotted as black dots. The size of the dot for the stabilizing solutes corresponds to the magnitude of the minimum solute concentration required to stabilize a grain size of 25 nm.

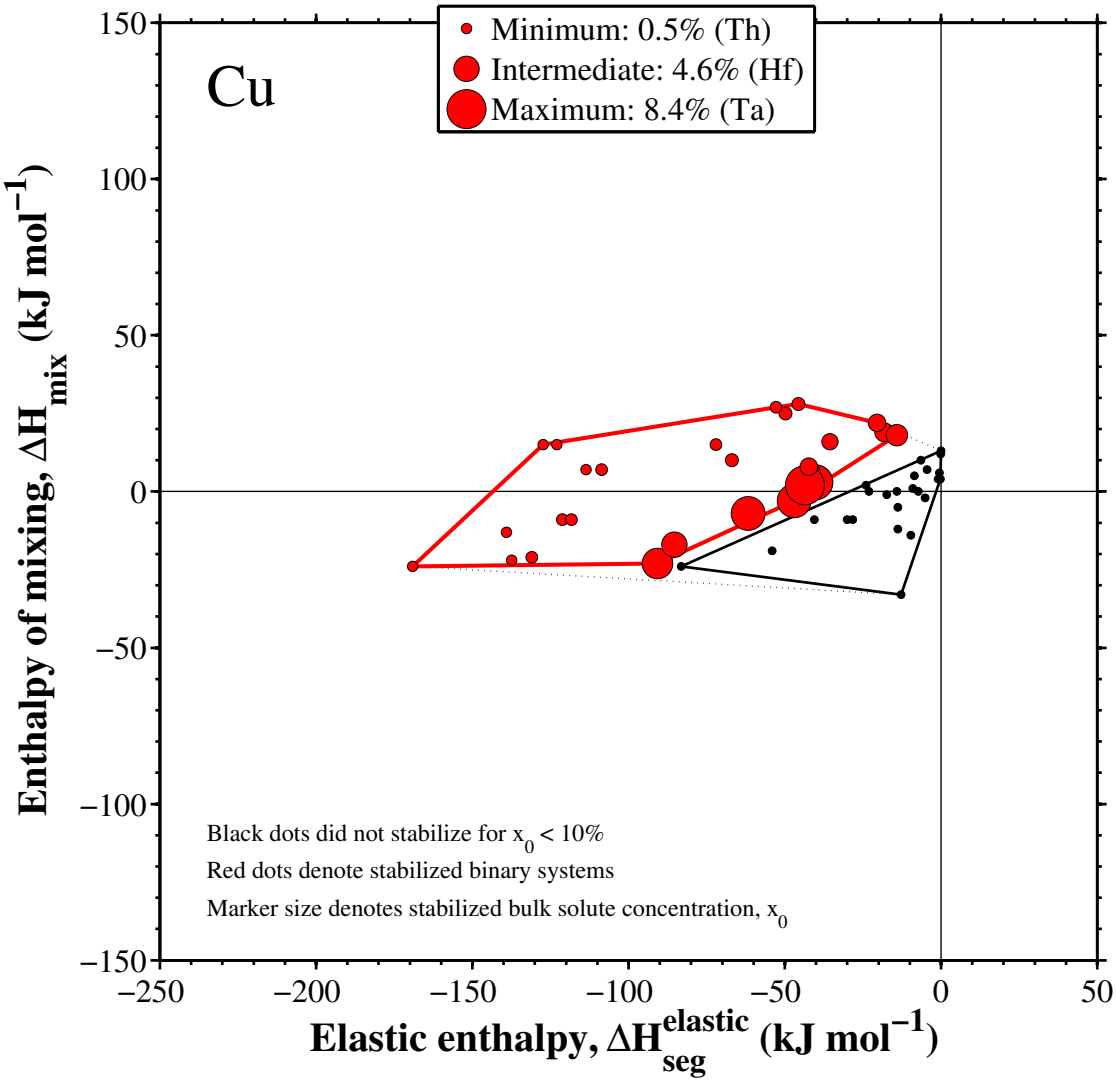

Figure 7. Nanocrystalline Cu stability map that plots the elastic enthalpy versus the enthalpy of mixing for both the stabilizing solutes (table 4, plotted as red dots) as well as the solutes that do not appear in table 4, plotted as black dots. The size of the dot for the stabilizing solutes corresponds to the magnitude of the minimum solute concentration required to stabilize a grain size of 25 nm.

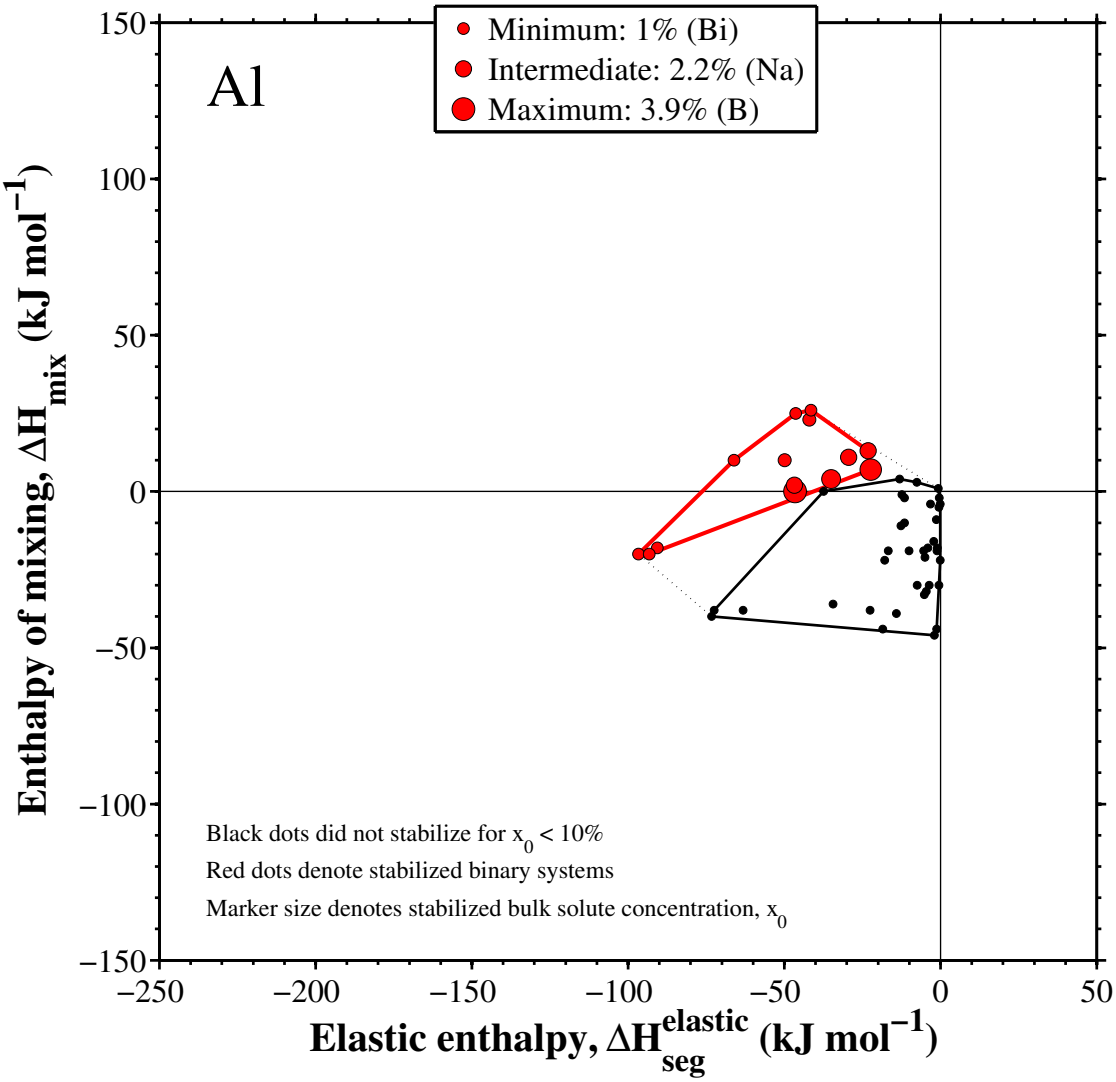

Figure 8. Nanocrystalline Al stability map that plots the elastic enthalpy versus the enthalpy of mixing for both the stabilizing solutes (table 5, plotted as red dots) as well as the solutes that do not appear in table 5, plotted as black dots. The size of the dot for the stabilizing solutes corresponds to the magnitude of the minimum solute concentration required to stabilize a grain size of 25 nm.

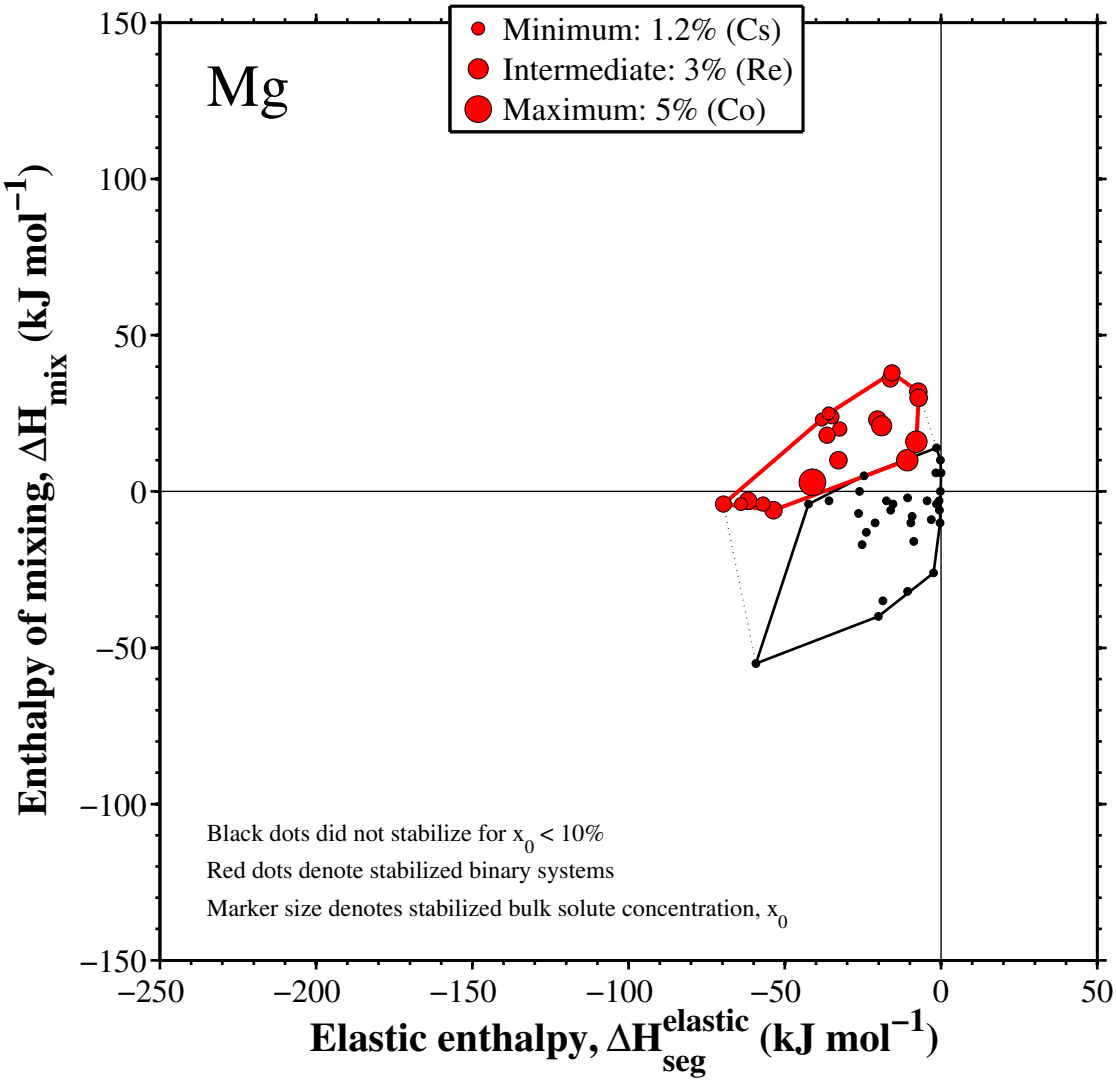

Figure 9. Nanocrystalline Mg stability map that plots the elastic enthalpy versus the enthalpy of mixing for both the stabilizing solutes (table 6, plotted as red dots) as well as the solutes that do not appear in table 6, plotted as black dots. The size of the dot for the stabilizing solutes corresponds to the magnitude of the minimum solute concentration required to stabilize a grain size of 25 nm.

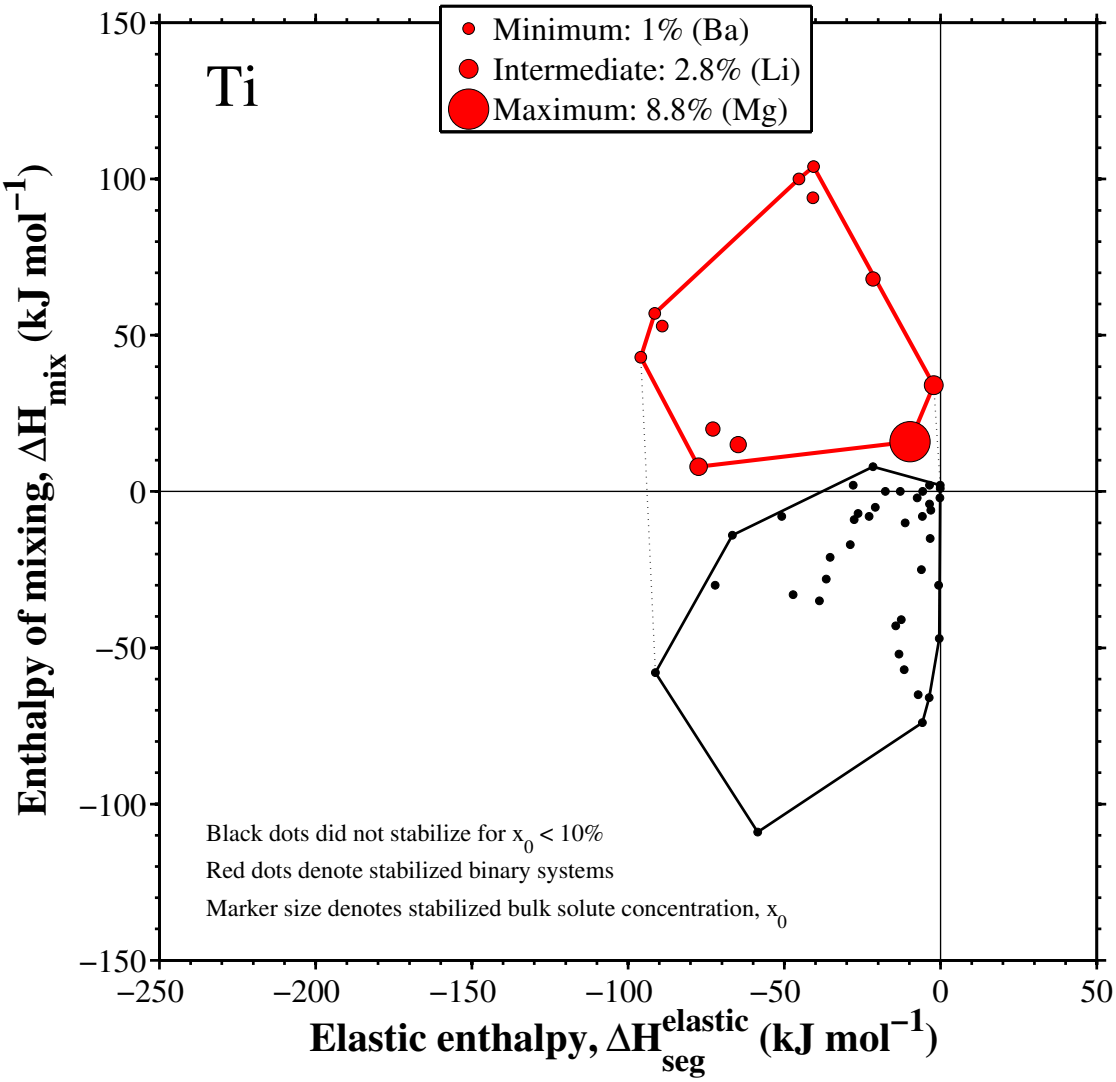

Figure 10. Nanocrystalline Ti stability map that plots the elastic enthalpy versus the enthalpy of mixing for both the stabilizing solutes (table 7, plotted as red dots) as well as the solutes that do not appear in table 7, plotted as black dots. The size of the dot for the stabilizing solutes corresponds to the magnitude of the minimum solute concentration required to stabilize a grain size of 25 nm.

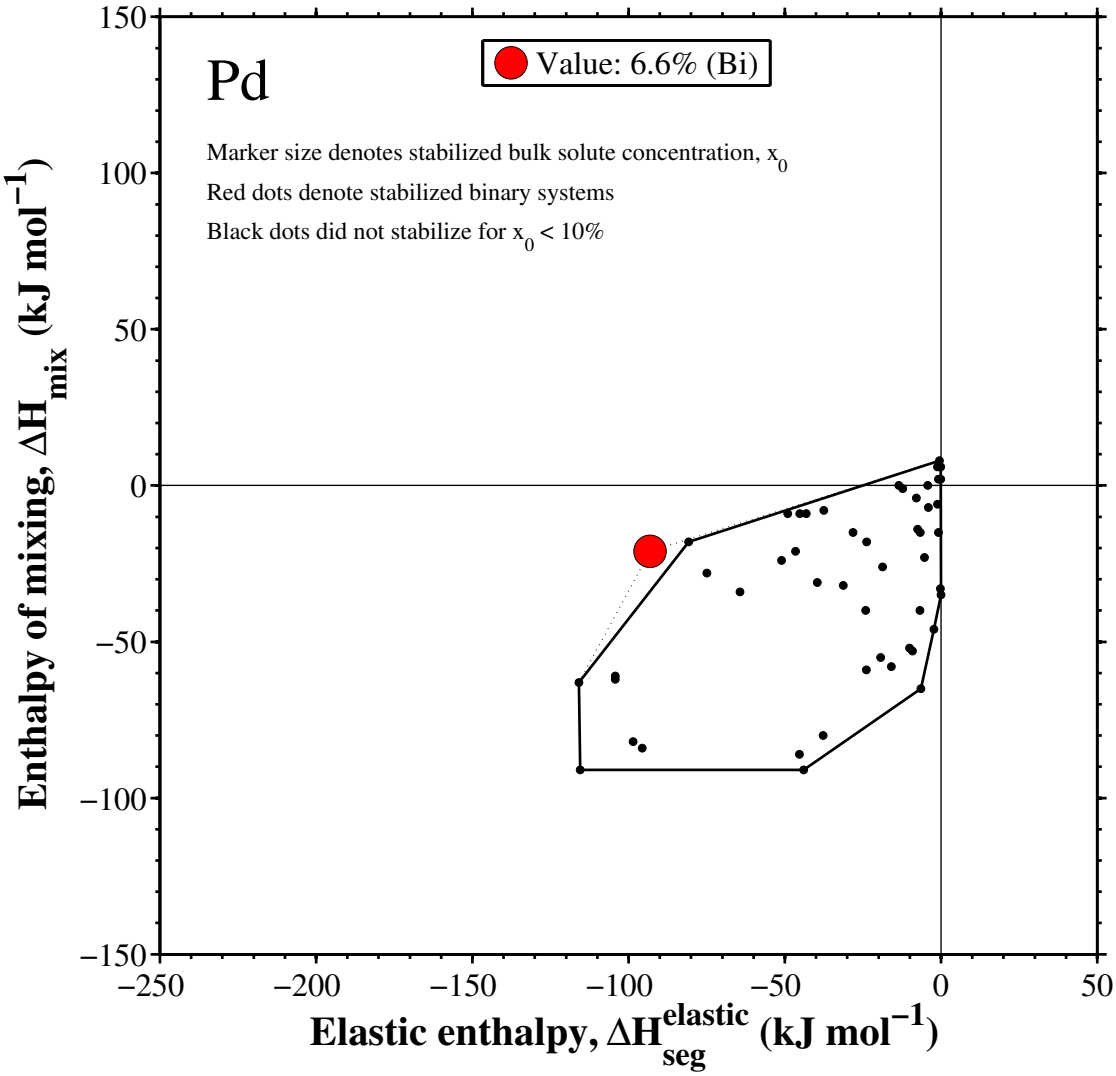

Figure 11. Nanocrystalline Pd stability map that plots the elastic enthalpy versus the enthalpy of mixing for both the stabilizing solutes (table 8, plotted as red dots) as well as the solutes that do not appear in table 8, plotted as black dots. The size of the dot for the stabilizing solutes corresponds to the magnitude of the minimum solute concentration required to stabilize a grain size of 25 nm.

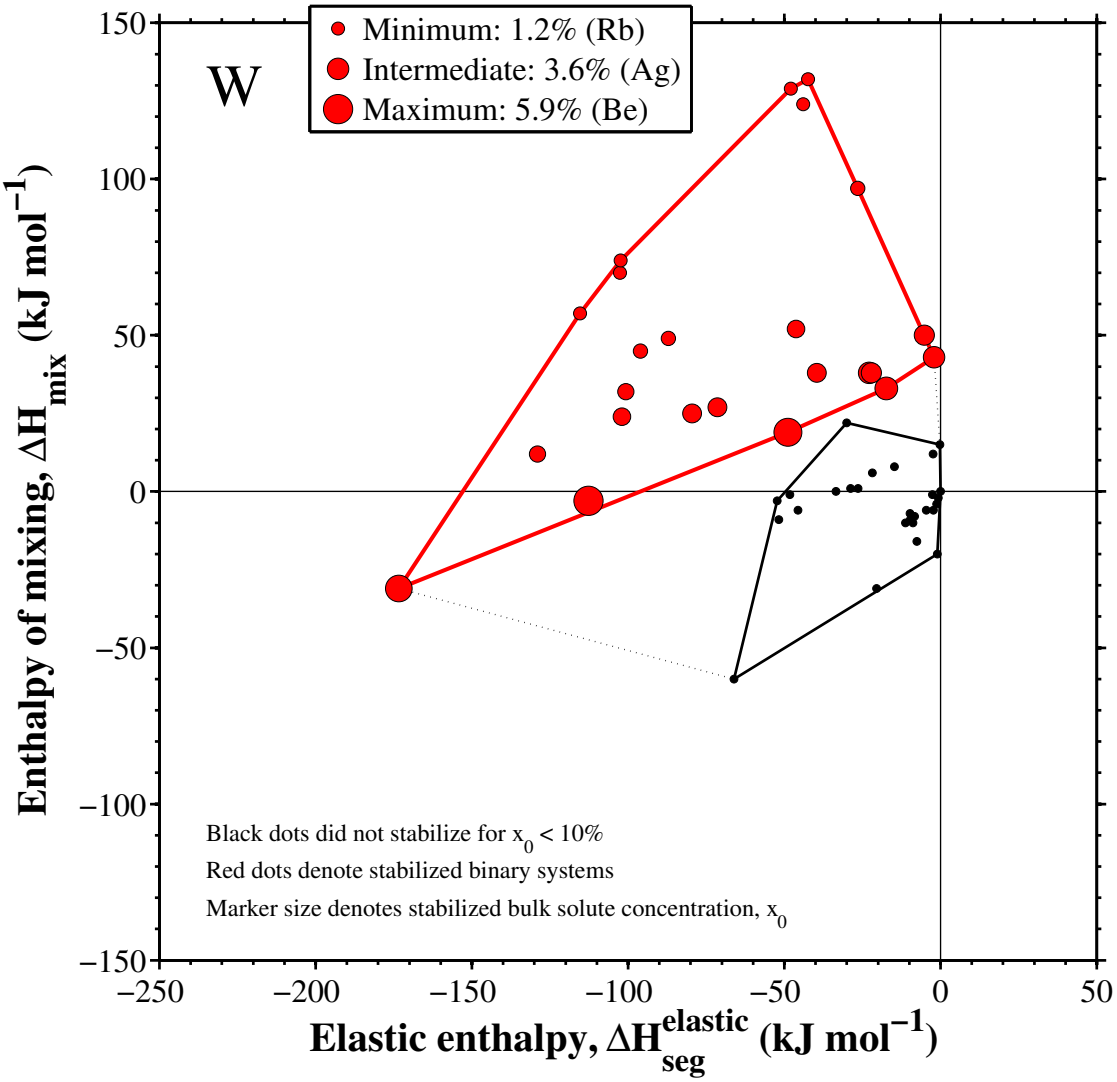

Figure 12. Nanocrystalline W stability map that plots the elastic enthalpy versus the enthalpy of mixing for both the stabilizing solutes (table 9, plotted as red dots) as well as the solutes that do not appear in table 9, plotted as black dots. The size of the dot for the stabilizing solutes corresponds to the magnitude of the minimum solute concentration required to stabilize a grain size of 25 nm.

Table 5. Solutes and their concentrations that stabilize the grain structure in nanocrystalline Al at temperature $T = 0.60T_M^{Al} = 396\,^{\circ}\mathrm{C}$ (669 K) and grain size $d_m = 25$ nm.

System (Al–X)	$\Delta H_{seg}^{elastic}$ (kJ mol^{-1})	ΔH_{mix} (kJ mol^{-1})	x_0 (at%)	Γ (μmol m^{-2})
Ca	-97	-20	1.0	7.1
Bi	-66	10	1.0	7.6
Rb	-46	25	1.1	8.5
Sr	-91	-18	1.1	7.7
Cs	-41	26	1.1	8.4
Ba	-93	-20	1.1	7.7
K	-42	23	1.2	9.2
Pb	-50	10	1.4	10.3
Sb	-47	2	2.0	13.6
Tl	-29	11	2.1	15.2
Na	-23	13	2.2	16.1
Sn	-35	4	2.8	18.5
In	-22	7	3.4	23.3
B	-47	0	3.9	20.7

Table 6. Solutes and their concentrations that stabilize the grain structure in nanocrystalline Mg at temperature $T = 0.60T_M^{Mg} = 389\,°\text{C}$ (662 K) and grain size $d_m = 25$ nm.

System (Mg–X)	$\Delta H_{seg}^{elastic}$ (kJ mol^{-1})	ΔH_{mix} (kJ mol^{-1})	x_0 (at%)	Γ (μmol m^{-2})
Rb	-38	23	1.2	6.5
Cs	-36	25	1.2	6.5
Ba	-64	-4	1.4	7.0
K	-32	20	1.5	8.1
Cr	-35	24	1.7	9.2
Sr	-57	-4	1.8	8.4
B	-70	-4	1.9	8.8
Mo	-16	36	1.9	10.5
W	-16	38	1.9	10.6
Fe	-36	18	2.0	10.6
Nb	-7	32	2.3	12.8
V	-20	23	2.4	13.0
Ca	-54	-6	2.5	10.0
Ta	-7	30	2.5	13.8
Be	-62	-3	2.6	10.8
Mn	-33	10	2.6	13.1
Re	-19	21	3.0	16.3
Na	-11	10	3.6	18.2
Ti	-8	16	3.7	19.8
Co	-41	3	5.0	19.7

Table 7. Solutes and their concentrations that stabilize the grain structure in nanocrystalline Ti at temperature $T = 0.60T_M^{Ti} = 996\,^{\circ}\text{C}$ (1269 K) and grain size $d_m = 25$ nm.

System (Ti–X)	$\Delta H_{seg}^{elastic}$ (kJ mol^{-1})	ΔH_{mix} (kJ mol^{-1})	x_0 (at%)	Γ (μmol m^{-2})
Rb	-45	100	1.0	7.4
Sr	-89	53	1.0	7.3
Cs	-41	104	1.0	7.4
Ba	-91	57	1.0	7.3
K	-41	94	1.1	8.1
Ca	-96	43	1.1	7.9
Na	-22	68	1.5	11.0
La	-73	20	1.8	12.3
Y	-65	15	2.2	14.6
Th	-77	8	2.3	14.7
Li	-2	34	2.8	19.8
Mg	-10	16	8.8	21.5

Table 8. Solutes and their concentrations that stabilize the grain structure in nanocrystalline Pd at temperature $T = 0.60T_M^{Pd} = 931\,^{\circ}\text{C}$ (1204 K) and grain size $d_m = 25$ nm.

System (Pd–X)	$\Delta H_{seg}^{elastic}$ (kJ mol^{-1})	ΔH_{mix} (kJ mol^{-1})	x_0 (at%)	Γ (μmol m^{-2})
Bi	-93	-21	6.6	14.6

Table 9. Solutes and their concentrations that stabilize the grain structure in nanocrystalline W at temperature $T = 0.60T_M^W = 2044\,°\text{C}$ (2317 K) and grain size $d_m = 25$ nm.

System (W–X)	$\Delta H_{seg}^{elastic}$ (kJ mol^{-1})	ΔH_{mix} (kJ mol^{-1})	x_0 (at%)	Γ (μmol m^{-2})
Rb	-48	129	1.2	9.7
K	-44	124	1.3	10.6
Cs	-42	132	1.3	10.6
Ba	-102	74	1.3	10.3
Ca	-115	57	1.4	11.0
Sr	-103	70	1.4	11.1
Na	-26	97	1.6	12.8
Pb	-87	49	1.8	13.8
Bi	-96	45	1.8	13.8
La	-101	32	2.0	14.8
Th	-129	12	2.2	15.2
Y	-102	24	2.3	16.6
Tl	-46	52	2.3	17.8
Sb	-80	25	2.7	19.3
Sn	-71	27	2.8	20.2
In	-40	38	2.9	21.7
Li	-5	50	3.0	23.2
Hg	-22	38	3.3	24.7
Mg	-23	38	3.4	25.6
Ag	-2	43	3.6	26.1
Cd	-17	33	4.1	25.8
B	-173	-31	5.0	14.3
Sc	-49	19	5.4	25.1
Be	-113	-3	5.9	22.1

3.3 Thermodynamic Stability Map Changes with Temperature

The thermodynamic stability plots were also plotted as a function of temperature for solutes in the Fe system (figure 13). In general, the plots do not change very much, aside from a solute or two. In this case, U is a stabilizing solute for Fe at low temperatures, but U is not predicted to be a stabilizing solute at concentrations below 10% for temperatures $T \geq 0.6T_m$. Hence, the bounds of the convex hull for stabilizing solutes shift towards solutes with higher enthalpy of mixing values and higher magnitudes of the elastic enthalpy. However, the bounds do not change drastically for this model.

Additionally, the nanocrystalline stability maps were plotted for the remaining systems at temperatures of $0.3T_m$ and $0.8T_m$. Thos plots are shown in figures 14 and 15. Again, a general trend is that the bounds of the convex hull for stabilizing solutes at higher temperatures shift towards solutes with higher enthalpy of mixing values and higher magnitudes of the elastic enthalpy. Clearly, the bounds for nonstabilizing solutes expands in this direction as well. Such thermodynamic stability maps can be used for help in selecting binary nanocrystalline alloys that are stable over a range of temperatures. Materials with applications at intermediate temperatures may be able to use different solutes for mitigating grain growth than applications at much higher temperatures. This information may also be combined with density, price, and embrittlement effect to aid in the selection of solutes for particular systems.

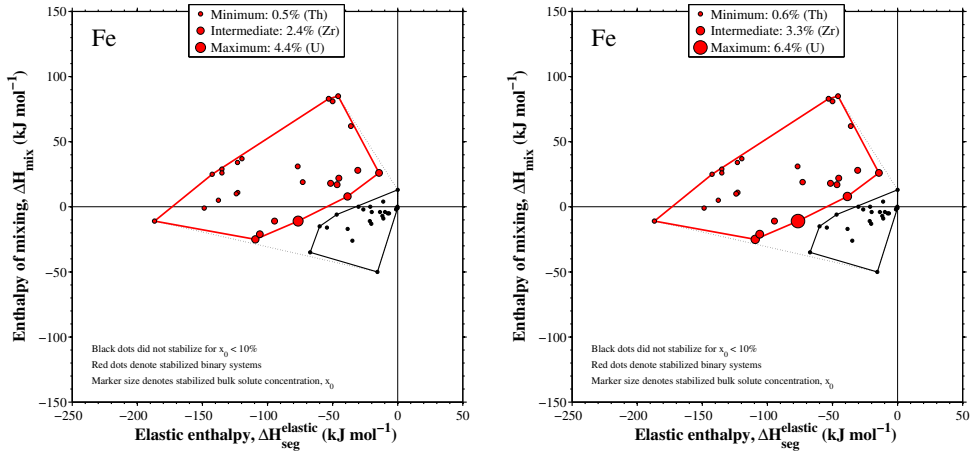

(a) $T = 0.3T_m = 733\,\mathrm{K}$

(b) $T = 0.4T_m = 887\,\mathrm{K}$

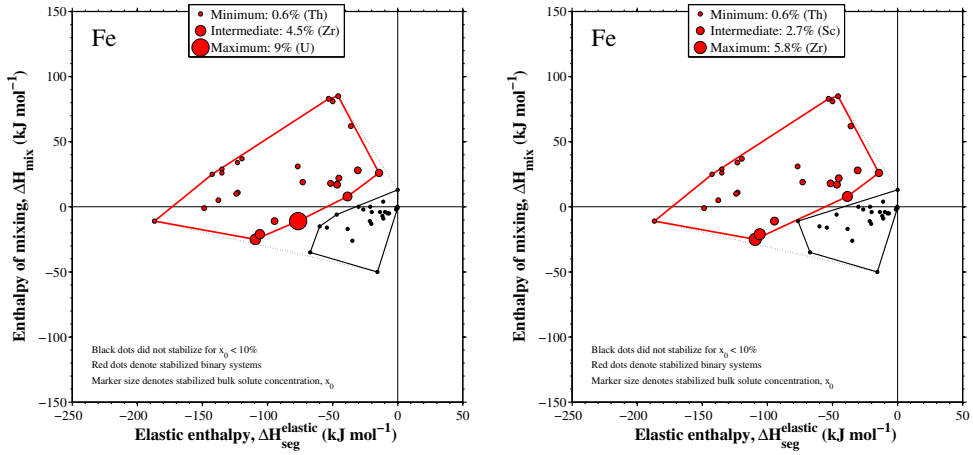

(c) $T = 0.5T_m = 1040\,\mathrm{K}$

(d) $T = 0.6T_m = 1194\,\mathrm{K}$

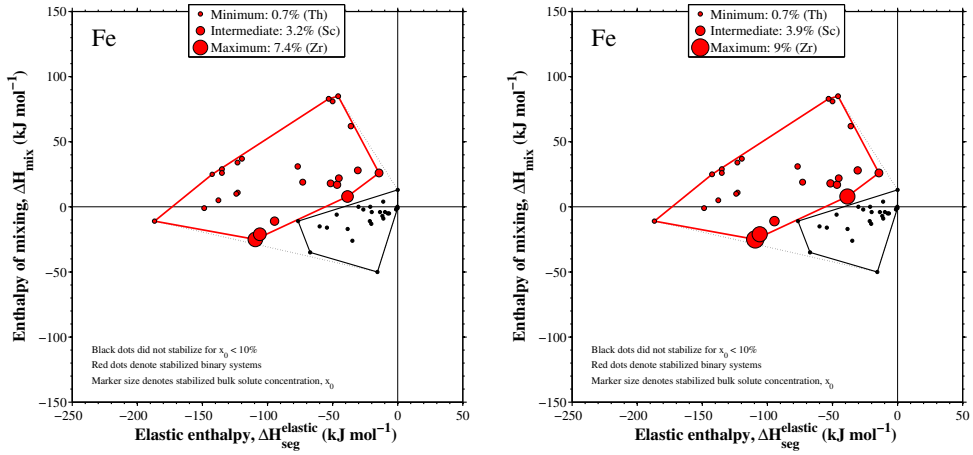

(e) $T = 0.7T_m = 1347\,\mathrm{K}$

(f) $T = 0.8T_m = 1501\,\mathrm{K}$

Figure 13. Nanocrystalline Fe stability maps as a function of temperature: (a) $0.3T_m$, (b) $0.4T_m$, (c) $0.5T_m$, (d) $0.6T_m$, (e) $0.7T_m$, and (f) $0.8T_m$. As temperature increases, the amount of solute required to stabilize the grain structure increases, up to the point that some solutes are effective at stabilizing at lower temperature, but are not effective for higher temperature stability (e.g., notice the large red dot for U at low temperatures shift to a black dot - nonstabilizing - at higher temperatures).

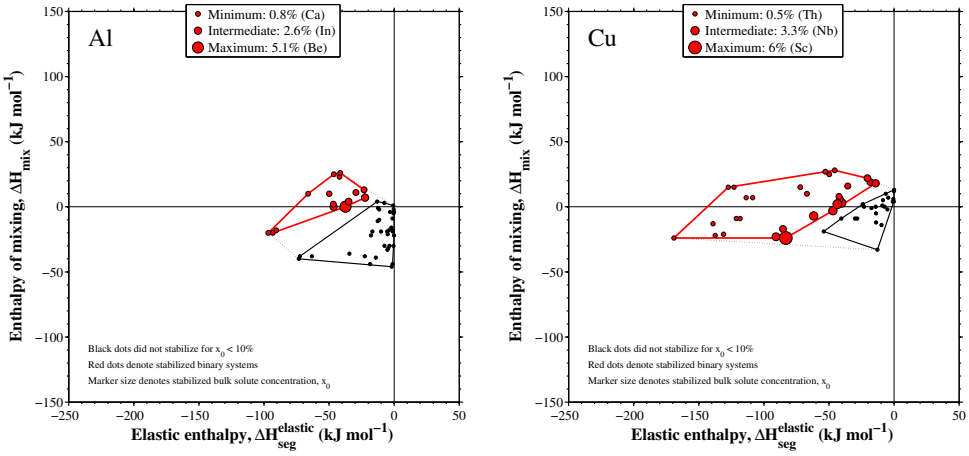

(a) $T = 0.3T_m$

(b) $T = 0.3T_m$

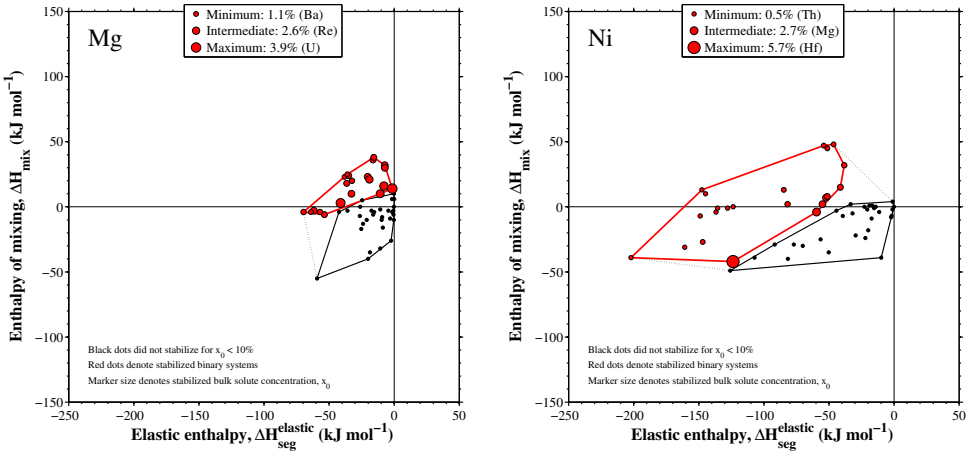

(c) $T = 0.3T_m$

(d) $T = 0.3T_m$

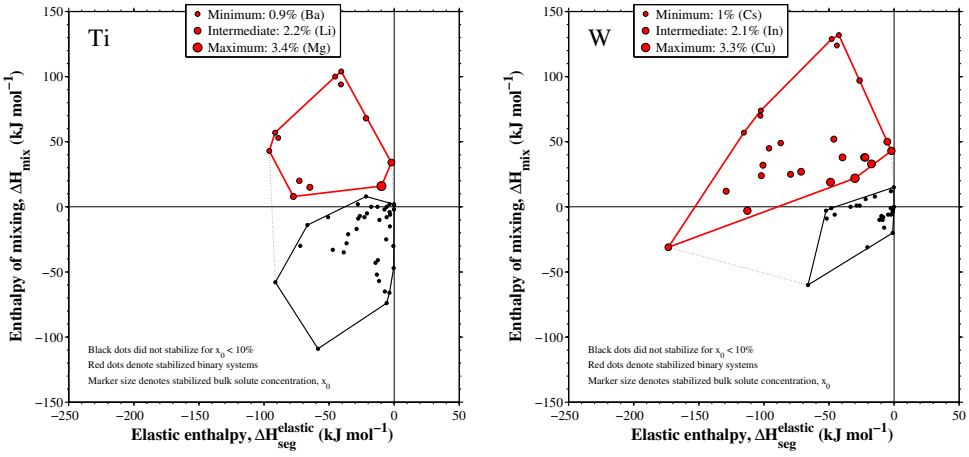

(e) $T = 0.3T_m$

(f) $T = 0.3T_m$

Figure 14. Nanocrystalline stability maps at $T = 0.3T_m$ for a number of elements: (a) Al, (b) Cu, (c) Mg, (d) Ni, (e) Ti, and (f) W.

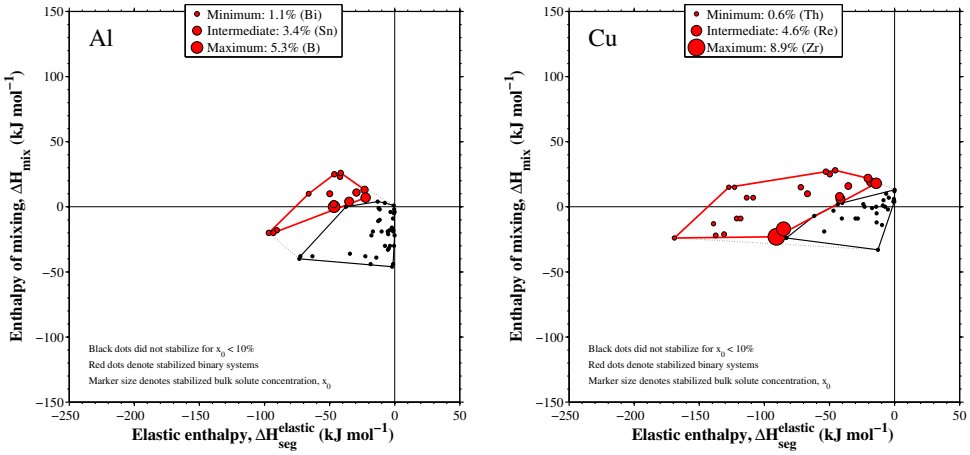

(a) $T = 0.8T_m$

(b) $T = 0.8T_m$

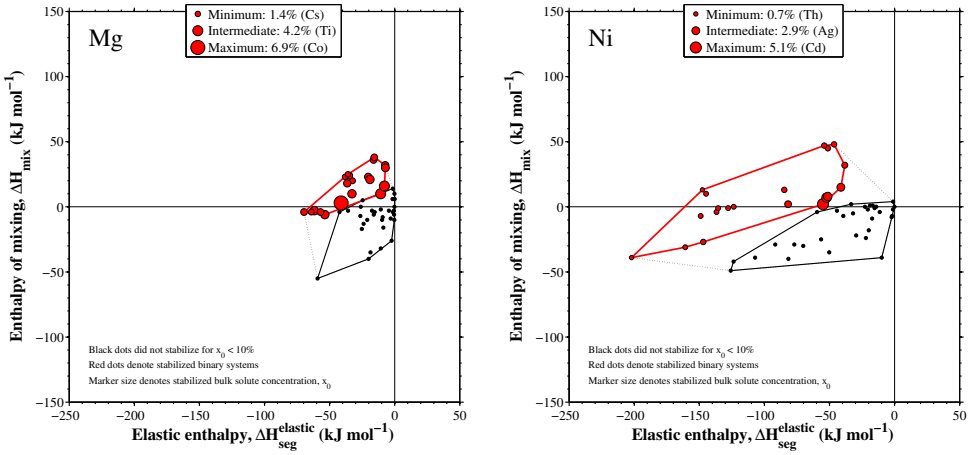

(c) $T = 0.8T_m$

(d) $T = 0.8T_m$

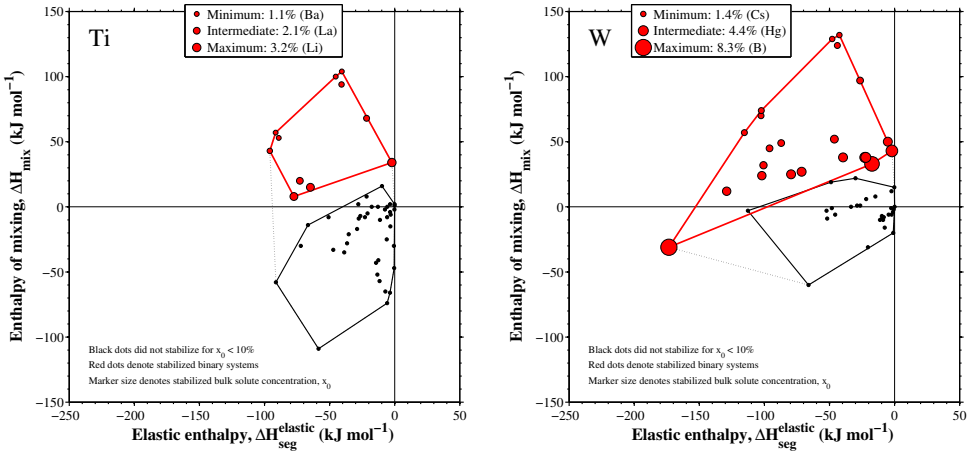

(e) $T = 0.8T_m$

(f) $T = 0.8T_m$

Figure 15. Nanocrystalline stability maps at $T = 0.8T_m$ for a number of elements: (a) Al, (b) Cu, (c) Mg, (d) Ni, (e) Ti, and (f) W.

3.4 Relationship between Solute Concentrations

The relationship between the bulk solute concentration, the grain boundary solute concentration and the grain interior solute concentration for all stabilized solvent-solute combinations (566 stabilized systems total from 1294 total systems) is discussed herein. There are a few trends that appear from examining these relationships.[†] As the bulk solute concentration required to stabliize the nanocrystalline grain structure increases, the concentration in the grain boundary increases as well (figure 16). In figure 16(a), notice that the grain boundary concentration increases dramatically as a function of this minimum bulk solute concentration; this trend suggests that there is a limit to the amount of bulk solute concentration that can be added to stabilize some systems. In figure 16(b), the grain interior solute concentration deviates from the 1:1 line drawn as solute segregates from the grain interior to the grain boundary, effectively resulting in a lower grain interior concentration. As the stabilized grain size increases, and grain boundary volume decreases, the solute concentration in the grain interior will approach the bulk solute concentration, i.e., less bulk solute concentration is required to stabilize the grain size.

The ratio between the solute concentration in the grain boundary and the grain interior changes as a function of the bulk solute concentration. Figure 17(a) plots the bulk solute concentration against the ratio of solute in the grain boundary to the grain interior for the stabilized systems at a grain size of $25\,\text{nm}$ and a temperature of $0.6T_M^A$ (T_M^A is the melting temperature of the corresponding solvent A). As the bulk solute concentration to stabilize the nanocrystalline grain structure increases, the ratio of solute concentration in the grain boundary to the grain interior decreases (figure 17). The solute concentration ratio axis in figure 17 is plotted on a log scale to highlight the large difference in this ratio as a function of bulk solute concentration. This sort of trend is as expected, i.e., the systems that stabilize at lower bulk solute concentrations do so because of a greater driving force for solute to segregate to the grain boundary and, hence, possess a higher ratio of solute in the boundary than the grain interior. Also, notice that the solute concentration ratio in this model is $>$10–100 times higher in the grain boundary than in the grain interior for most systems, which may dramatically impact properties. Figure 17(b) shows these same systems for several different stabilized grain sizes. First, as the stabilized grain size increases, the ratio of solute concentration in the grain boundary to the grain interior increases dramatically for those systems that require a low bulk solute concentration for stabilization. This result has to do with the rapid decrease in grain boundary volume with increasing grain size combined with a reduced amount of bulk solute required to stabilize the grain structures, which is

[†]There are a few systems that appear to be outliers from the general trends. For instance, the two systems above the 1:1 line in figure 16(b) are the K–Pt and Cs–Pt systems. In figure 17, there were multiple systems that were removed as outliers: K–Pt, Cs–W, Cs–Re, Cs–Os, Cs–Ir, Cs–Pt.

more pronounced in the dilute limit. By comparison, at larger bulk solute concentrations, there is a much smaller difference in this ratio as a function of the stabilized grain size.

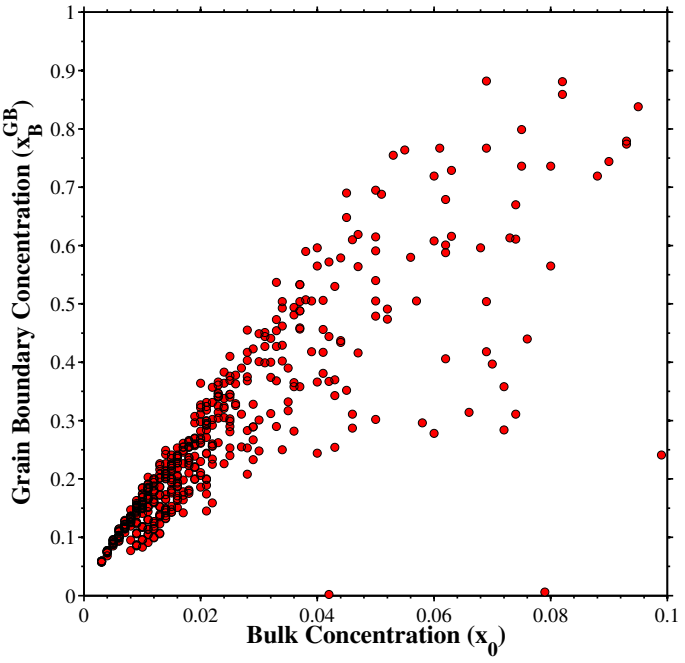

(a)

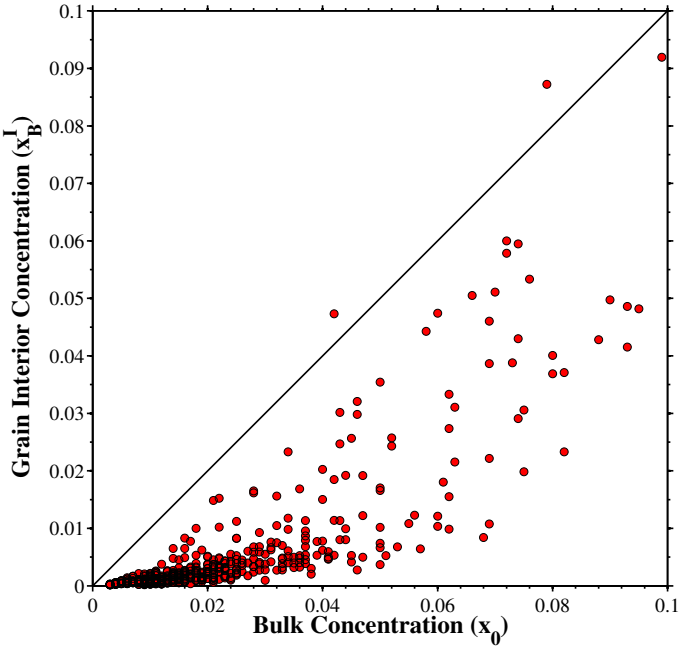

(b)

Figure 16. (a) Grain boundary solute concentration x_B^{GB} and (b) grain interior solute concentration x_B^I as a function of the minimum bulk solute concentration required to stabilize the nanocrystalline grain size at a grain size of 25 nm and a temperature of $0.6T_M^A$ (T_M^A is the melting temperature of the corresponding solvent A).

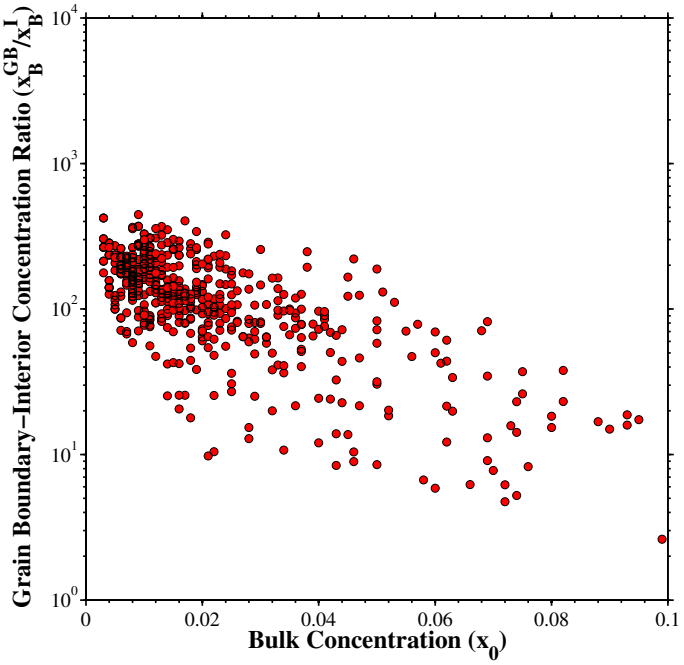

(a)

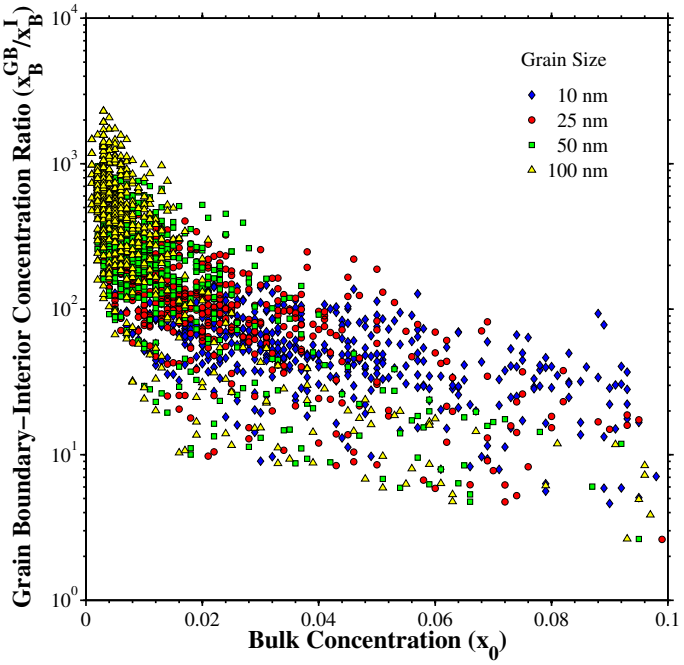

(b)

Figure 17. The ratio of the solute concentration in the grain boundary to the grain interior as a function of the bulk solute concentration for stabilized nanocrystalline systems at a temperature of $0.6T_M^A$ for (a) a stabilized grain size of 25 nm and (b) stabilized grain sizes of 10, 25, 50 and 100 nm.

4. Summary and Conclusions

A fundamental thermodynamic analysis is performed for the change in grain boundary energy that results from solute segregation to grain boundaries in a closed system. When the grain boundary energy is reduced to zero, the grain size can be stabilized against further change. The theoretical results provide a detailed picture of the stabilization effects. The developed model and stability maps aid in selecting binary systems that will open new regimes in processing, manufacturing and applications space. Specific findings of the present work include:

1. A methodology and model for thermodynamic stabilization of nanocrystallinity is presented. This thermodynamic-based model allows for the prediction of a large number of individual binary systems.

2. Numerical calculations were made for the Fe–Zr system, demonstrating that thermodynamic stabilization for nanoscale grain sizes can be expected in Fe–Zr alloys up to $900\,^{\circ}\mathrm{C}$ for Zr contents on the order of 4 at% Zr (figures 3–4). This is in good agreement with the experimental observations.

3. A thermodynamic stability map was made for Fe-based systems. A strong effect of enthalpy of mixing is revealed in the calculations (figure 5). We conclude that in appropriate alloy systems with suitable values of elastic and mixing enthalpy of segregation, thermodynamic stabilization of a nanoscale grain size is possible up to high homologous temperatures.

4. The utility and universality of this model are demonstrated by applying it to over 2000 binary systems. Herein, we applied this to Fe, Ni, Cu, Al, Mg, Ti, Pd, and W (tables 2–9) However, these maps must be balanced with other properties, e.g., secondary phase formation, solubility limit, and grain boundary embrittlement must be considered as well.

5. References

1. Weissmuller, J. Alloy thermodynamics in nanostructures. *J. Mater. Res.* **1994**, *9 (1)*, 4–7.

2. Weissmuller, J. Alloy effects in nanostructures. *Nanostruct. Mater.* **1993**, *3 (1–6)*, 261–272.

3. Krill, C. E.; Ehrhardt, H.; Birringer, R. Thermodynamic stabilization of nanocrystallinity. *Z. Metallkd.* **2005**, *96 (10)*, 1134–1141.

4. Detor, A. J.; Schuh, C. A. Grain boundary segregation, chemical ordering and stability of nanocrystalline alloys: Atomistic computer simulations in the Ni-W system. *Acta Mater.* **2007**, *55 (12)*, 4221–4232.

5. Beke, D. L.; Cserhati, C.; Szabo, A. Segregation inhibited grain coarsening in nanocrystalline alloys. *J. Appl. Phys.* **2007**, *95 (9)*, 4996–5001.

6. Kirchheim, R. Grain coarsening inhibited by solute segregation. *Acta Mater.* **2002**, *50 (2)*, 413–419.

7. Kirchheim, R. Reducing grain boundary, dislocation line and vacancy formation energies by solute segregation. I. Theoretical background. *Acta Mater.* **2007**, *55 (15)*, 5129–5138.

8. Trelewicz, J. R.; Schuh, C. A. Grain boundary segregation and thermodynamically stable binary nanocrystalline alloys. *Phys. Rev. B* **2009**, *79 (9)*, 1–13.

9. Darling, K. A.; VanLeeuwen, B. K.; Koch, C. C.; Scattergood, R. O. Thermal stability of nanocrystalline Fe–Zr alloys. *Mater. Sci. Eng. A* **2010**, *527 (15)*, 3572–3580.

10. Darling, K. A.; VanLeeuwen, B. K.; Semones, J. E.; Koch, C. C.; Scattergood, R. O.; Kecskes, L. J.; Mathaudhu, S. N. Stabilized nanocrystalline iron-based alloys: Guiding efforts in alloy selection. *Mater. Sci. Eng. A* **2011**, *528 (13–14)*, 4365–4371.

11. VanLeeuwen, B. K.; Darling, K. A.; Koch, C. C.; Scattergood, R. O.; Butler, B. G. Thermal stability of nanocrystalline $Pd_{81}Zr_{19}$. *Acta Mater.* **2011**, *58 (12)*, 4292–4297.

12. Wynblatt, P. W.; Chatain, D. Anisotropy of segregation at grain boundaries and surfaces. *Metall. Mater. Trans. A* **2006**, *37 (9)*, 2595–2620.

13. Hillert, M. *Phase equilibria, phase diagrams and phase transformations: Their thermodynamic basis*; 2^{nd} ed.; Cambridge University Press: New York, 2008.

14. Sutton, A. P.; Balluffi, R. W. *Interfaces in crystalline materials*; Oxford University Press: USA, 1997.

15. Wynblatt, P.; Ku, R. C. Surface energy and solute strain energy effects in surface segregation. *Surf. Sci.* **1977**, *65 (2)*, 511–531.

16. deBoer, F. R.; Boom, R.; Mattens, W. C. M.; Miedema, A. R.; Niessen, A. K. *Cohesion in metals: Transition metal alloys, Vol 1. Cohesion and structure*; Elsevier Scientific: Amsterdam, 1988.

17. Takeuchi, A.; Inoue, A. Classification of bulk metallic glasses by atomic size difference, heat of mixing and period of constiuent elements and its application to characterization of the main alloying element. *Mater. Trans. JIM* **2005**, *46 (12)*, 2817–2829.

18. Friedel, J. Electronic structure of primary solid solutions in metals. *Adv. Phys.* **1954**, *3 (12)*, 446–507.

19. Eshelby, J. D. The force on an elastic singularity. *Phil. Trans. R. Soc. Lond. A* **1951**, *244 (877)*, 87–112.

20. Saber, M.; Kotan, H.; Koch, C. C.; Scattergood, R. O. Thermodynamic stabilization of nanocrystalline binary alloys. *J. Appl. Phys.* **2013**, *113*, 063515.

21. Tyson, W. R.; Miller, W. A. Surface free energies of solid metals: Estimation from liquid surface tension measurements. *Surf. Sci.* **1977**, *62 (1)*, 267–276.

22. Vitos, L.; Ruban, A. V.; Skriver, H. L.; Kollar, J. The surface energy of metals. *Surf. Sci.* **1998**, *411 (1–2)*, 186–202.

23. Cardarelli, F. *Materials handbook: A concise desktop reference*; 2^{nd} ed.; Springer-Verlag: London, 2008.

24. Koch, C. C.; Scattergood, R. O.; Darling, K. A.; Semones, J. E. Stabilization of nanocrystalline grain sizes by solute additions. *J. Mater. Sci.* **2008**, *43 (23–24)*, 7264–7272.

25. Seah, M. P. Grain boundary segregation. *J. Phys. F. Metal. Phys.* **2008**, *10*, 1043–1064.

26. Dowben, P. A.; Miller, A. *Surface segregation phenomena*; CRC Press Inc.: Boca Raton, Florida, 1990.

27. Pellicer, E.; Varea, A.; Sivaraman, K. M.; Pané, S.; Suriñach, S.; Baró, M. D.; Nogués, J.; Nelson, B. J.; Sort, J. Grain Boundary Segregation and Interdiffusion Effects in Nickel–Copper Alloys: An Effective Means to Improve the Thermal Stability of Nanocrystalline Nickel. *ACS Appl. Mater. Inter.* **2011**, *3 (7)*, 2265–2274.

28. Frolov, T.; Darling, K. A.; Kecskes, L. J.; Mishin, Y. Stabilization and strengthening of nanocrystalline copper by alloying with tantalum. *Acta Mater.* **2012**, *60*, 2158–2168.

29. Atwater, M. A.; Scattergood, R. O.; Koch, C. C. The stabilization of nanocrystalline copper by zirconium. *Mater. Sci. Eng. A* **2013**, *559*, 250–256.

NO. OF COPIES	ORGANIZATION
1 (PDF)	DEFENSE TECHNICAL INFORMATION CTR DTIC OCA
2 (PDF)	DIRECTOR US ARMY RESEARCH LAB RDRL CIO LL IMAL HRA MAIL & RECORDS MGMT
1 (PDF)	GOVT PRINTG OFC A MALHOTRA

NO. OF COPIES	ORGANIZATION
1 (PDF)	US ARMY RESEARCH LABORATORY RDRL WMM J ZABINSKY R DOWDING
1 (PDF)	US ARMY RESEARCH LABORATORY RDRL WMM F M TSCHOPP K DARLING H MURDOCH L KECSKES H MAUPIN
1 (PDF)	US ARMY RESEARCH LABORATORY RDRL WML H J NEWILL T EHLERS
1 (PDF)	MILLERSVILLE UNIVERSITY M ATWATER
1 (PDF)	PENN STATE UNIVERSITY ZK LIU B VANLEEUWEN